RESEARCH ARTICLE

WILEY

Simultaneously iterative procedure based on block Newton method for elastoplastic problems

Takeki Yamamoto[1] | Takahiro Yamada[2] | Kazumi Matsui[2]

[1]Department of Aerospace Engineering, Tohoku University, Sendai, Miyagi, Japan

[2]Graduate School of Environment and Information Science, Yokohama National University, Yokohama, Kanagawa, Japan

Correspondence
Takeki Yamamoto, Department of Aerospace Engineering, Tohoku University, Aza-Aoba 6-6-01, Aramaki, Aoba-ku, Sendai, Miyagi 980-8579, Japan.
Email: takeki.yamamoto.c2@tohoku.ac.jp

Abstract

In this article, the authors formulate elastoplastic problems as a coupled problem of the equilibrium equation and the yield condition at each material point, and develop a numerical procedure based on the block Newton method to solve the overall structure using the finite element discretization. For the integration of stress, the backward difference scheme is employed. In the conventional return mapping algorithm, the algorithmic tangent moduli are derived analytically so that it is consistent with local iterative calculation to determine internal variables. On the other hand, in the proposed block Newton method, the tangent moduli can be obtained algebraically by eliminating the internal variables, and the internal variables are also updated algebraically without local iterative calculation. The residual of the yield condition is incorporated into the linearized equilibrium equation. The proposed approach enables the errors of the equilibrium equation and the yield condition to decrease simultaneously. Some numerical examples show the validity and effectiveness of the proposed approach by comparing the results of the proposed approach with those of the conventional return mapping algorithm.

KEYWORDS

backward difference scheme, block Newton method, elastoplasticity, finite element analysis, small strains

1 | INTRODUCTION

The problem of structures considering material nonlinearity is determined by two different mechanical behaviors of the deformation in the structure and the nonlinear response of materials. The structural deformation is governed by the equilibrium equation usually expressed in terms of displacement. In elastoplasticity, the evolution of the plastic strain is based on the yield condition, which depends on the stress state and a set of internal variables. Hence, the elastoplastic problems can be formulated as a coupled problem to determine displacement fields in the structures and internal variables of materials.

The basic structure of rate-independent plasticity is outlined within the classical framework of response functions formulated in stress space.[1,2] In the formulations, the loading/unloading conditions in the so-called Kuhn–Tucker form have been the standard complementarity conditions for constrained problems subject to unilateral constraints. This form of the loading/unloading conditions is classical and has been used by several authors.[2-4] Since the algorithmic elastoplastic problem is typically formulated in strain space, the strain tensor is regarded as the primary (driving) variable. This standard point of view adopted in the numerical analysis has been proposed by the pioneering work of Wilkins.[5]

The inelastic behavior of rate-independent elastoplasticity is expressed in the incremental form characterized by the rate-dependent constitutive equation. The radial return algorithm, which is proposed by Wilkins,[5] has been the most widely used integration procedure for plane strain and three-dimensional classical J_2 plasticity. The representative algorithm is extended to account for linear isotropic and kinematic hardening by Krieg and Key.[6] Krieg and Krieg[7] proposed alternative formulations of elastic predictor/plastic corrector methods. It should be noted that the radial return algorithms have been often employed in conjunction with the so-called elastoplastic tangent. These elastoplastic moduli are obtained from the "continuum" rate constitutive model by enforcement of the consistency condition. However, the procedure results in loss of the quadratic rate of asymptotic convergence particularly important for large time steps.[8]

The return mapping algorithms[9] have been developed to express a purely elastic trial state followed by a plastic corrector phase. Note that the return mapping algorithms cover the radial return algorithm, which is applied in a particular case of elastic predictor/plastic corrector approach. To a large extent, the return mapping algorithms have replaced older treatments based on the elastoplastic tangent modulus, as in Nayak and Zienkiewicz[10] or Owen and Hinton.[9] Within the framework of this class of algorithms, Simo and Taylor[11] presented a systematic procedure whereby for rate-independent plasticity. To realize the desired property of iterative solution scheme, they developed an explicit expression for the tangent moduli consistent with the integration algorithm. In the consistent approach,[11] an effective and robust integration scheme is applied to the rate-dependent constitutive equation by the return mapping algorithm,[5,9] and the consistency condition, which was firstly proposed by Wilkins,[5] is discretely imposed. Hence, by applying a consistent method between the tangent coefficients and the integration algorithms, an asymptotic quadratic convergence is attained in the iterative solution scheme based on the Newton method.

Approaches which improve the rate of convergence in the elastoplastic analysis by the finite element method have been proposed, since it is obvious that the consistent approach exhibits only the asymptotic quadratic convergence. Braudel et al.[12,13] derived the rate-dependent formulation combining the principle of virtual work with the implicit incremental form of the constitutive equation. They constructed a linear system of equations with the equilibrium equation of the overall structure and the yield condition at integration points. Hence, the resulting linear system of equations are obtained by static condensation of the internal variables. Note that, in these approaches, the local unknowns at integration points contain the increments of the stress tensor, the strain tensor, the plastic strain tensor, and the consistency parameter. On the other hand, Riggs[14] proposed a substructure analogy to describe the plastic deformation for nonlinear structural analysis. In this approach, a substructure stiffness matrix can be derived by condensing the additional internal variables, which represent the plastic deformation, out with the stress–strain relation. Martin et al.[15] expressed the increment of strain energy by the increments of displacement and internal slip, and introduced the dissipation function into the energy function corresponding to displacement and slip. Based on this idea, the linear system of equations is written using the degrees of freedom of displacement and those of slip. This approach also leads to the internal variable formulation proposed by Reddy et al.[16] The internal variable formulation is an approach to solve both the equilibrium equation of the overall structure and the condition imposed on internal variables. In this approach, the dissipation function corresponding to the evolution of plasticity is added to the definition of the free energy function; hence, the formulation can be directly applied to the incremental form in the numerical analysis. In the situation of plane stress for elastoplastic problems, de Borst[17] introduced the transverse normal strain as the internal variable for satisfying the plane stress condition. In this formulation, the transverse normal stress is not necessarily zero for each of the iterations. Hence, the proper tangent moduli and the consistent internal force vectors for a plane stress situation can be obtained using the incremental form of the transverse normal stress. Note that the residual of the transverse normal stress is incorporated into the internal force vectors. Considering the importance of the mechanical formulations, these numerical algorithms have been employed in practical situation.[18-20] Thus, the mechanical approach using the path independent scheme is extended to the field of the sensitivity analysis.[21-23] In addition, in the field of the multiscale analysis, the efficient tangent coefficient can be constructed focusing on between the degrees of freedom in the microscale and those in the macroscale.[24] For a quadratic cone complementation problem, Zhang et al.[25] presented the tangent coefficient for solving the equilibrium equation by expressing the stress state at the Gauss integration point only by internal variables. Fritzen and Hassani[26] suggested the space–time approach for calculating the displacements and the internal variables simultaneously in both the full model as well as the reduced order one, similarly to the study by Miehe.[27] On the other hand, in the field of fluid–structure interaction, the strong coupling, where equilibrium between fluid and structure is satisfied jointly, is performed in each time step by using the block Newton method.[28,29]

In the numerical algorithm for nonlinear equations, the rate of convergence by using the Newton method has been emphasized. Chaboche and Cailletaud[30] proposed the integration procedure for the constitutive model that needs special numerical treatments when a large number of internal variables contains. In this investigation, several options including both implicit and explicit integration approaches have been compared through numerical tests. From the material model described nonlinear rate-dependent,[30] a system of differential–algebraic equations is constructed with both the discretized form of the principle of virtual work and the ordinary differential equations of the constitutive model defined locally at integration points. Based on this formulation, Ellsiepen and Hartmann[31] developed the solution scheme with the diagonally implicit Runge–Kutta methods for updating the displacements and the internal variables simultaneously. In this approach, the internal variables are updated using local iterative calculations for fulfilling each algebraic equation, and then the displacements are calculated to satisfy the equilibrium equation. Here, the convergence is checked by substituting the updated displacements and internal variables into each algebraic equation and the equilibrium equation. Hence, the global iterative calculation is repeated until the solutions have sufficiently converged. Therefore, in each iteration, the residuals of the algebraic equations are not incorporated into the residual of the equilibrium equation. By using this approach, it is possible to control step size of time integration procedures for differential–algebraic equations. However, the tangent stiffness matrix is lost of the advantage of a band-structured sparse matrix. They employed the Multilevel-Newton algorithm to overcome this disadvantage. On the other hand, Eckert et al.[32] treated not only the displacements but also the internal variables involved in elastoplasticity as the global degrees of freedom, similarly to the study by Scherf and Simeon;[33] hence, in their formulation, the whole set of equations is linearized. In this numerical scheme, all quantities are solved and updated at the end of each iteration step simultaneously. To allow automatic time step size control, a predictor is employed for the displacements giving initial values at the beginning of each time step. In this approach, the residuals of all equations are independently considered. These monolithic schemes applied higher order time integration have been extended to viscoelasticity,[34-36] elastoplasticity,[37] and viscoplasticity.[38-41] In addition, Hartmann[42] reported the rate of convergence of the general Multilevel-Newton algorithm in nonlinear finite element analysis based on the quasi-static problem of solid mechanics for elastoplastic problems, and tried to improve the convergence of the Multilevel-Newton algorithm by deriving the linear system of equations including internal variables. Ekh and Menzel[43] investigated the convergence of the Newton method in the case of the structures modeled by the complicated constitutive laws, and pointed out the importance of the numerical algorithm for the nonlinear equation in the implicit integration algorithm. Similarly, the studies of stress integration algorithms for the rate of convergence have been addressed extensively. To offer more accurate solutions with a high precision on the conservation of yield condition for a long term calculation, Liu[44] suggested the numerical procedure as a combination of the Lie group method and the Newton method to solve a system of differential–algebraic equations.

In this work, we formulate elastoplastic problems as a coupled problem of the equilibrium equation and the yield condition at each material point, and develop a numerical procedure based on the block Newton method to solve the overall structure using the finite element discretization. By virtue of this idea, the consistency parameter, which is the internal variable for expressing the evolution of the plasticity, can be condensed out from the incremental form of the equilibrium equation at each material point. In the conventional return mapping algorithm, the algorithmic tangent moduli are derived analytically so that it is consistent with local iterative calculation to determine the consistency parameter.[45,46] On the other hand, in the proposed approach, the tangent moduli can be obtained algebraically by eliminating the internal variables, and the internal variables are also updated algebraically without local iterative calculation. In addition, the residual of the yield condition is incorporated into the linearized equilibrium equation. The incremental form of the equilibrium equation for the overall structure can be solved by the standard procedure using the finite element discretization, similarly to the conventional return mapping algorithm. In the proposed formulation, rate-independent J_2 plasticity is adopted.

Some representative numerical examples are presented to verify the proposed approach. As examples, two-dimensional models in plane strain state are solved. We focus on the number of iterations, the rate of convergence, and the behavior of the residual norm for convergence to evaluate the robustness and effectiveness of the proposed approach.

2 | CLASSICAL RATE-INDEPENDENT PLASTICITY

In this section, we summarize below the governing equations of classical rate-independent plasticity within the context of the three-dimensional infinitesimal theory.[45,46] Throughout this discussion, no explicit indication of the arguments in a field is made.

2.1 | Local evolution equations

The fields $\boldsymbol{u}$, $\boldsymbol{\varepsilon}$, and $\boldsymbol{\sigma}$ are evaluated at a point $\boldsymbol{x} \in \Omega$, which is the reference placement of a continuum body, and current time t is often taken as the entire $\mathbb{R}_+$ for convenience. In addition, we denote the strain history at a point $\boldsymbol{x} \in \Omega$ up to current time $t \in \mathbb{R}_+$.

From a phenomenological point of view, we regard plastic flow as an irreversible process in materials, typically metals, characterized in terms of the history of the strain tensor $\boldsymbol{\varepsilon}$ and two additional variables: the plastic strain $\boldsymbol{\varepsilon}^{\mathrm{p}}$ and a suitable set of $n_{\mathrm{iv}} \geq 0$ internal variables generically denoted by $\boldsymbol{\alpha}$ and often referred to as hardening parameters. In a strain-driven formulation, plastic flow at each point $\boldsymbol{x} \in \Omega$ up to current time $t \in \mathbb{R}_+$ is represented in terms of $\boldsymbol{\varepsilon}, \boldsymbol{\varepsilon}^{\mathrm{p}}$, and $\boldsymbol{\alpha}$. In this context, the stress tensor is a dependent function of the variables $(\boldsymbol{\varepsilon}, \boldsymbol{\varepsilon}^{\mathrm{p}})$ through the elastic stress–strain relations, as discussed below. This leads to a strain space formulation of plasticity. Even though, we regard $\{\boldsymbol{\varepsilon}, \boldsymbol{\varepsilon}^{\mathrm{p}}, \boldsymbol{\alpha}\}$ as the independent "driving" variables, in the response functions in classical plasticity, that is, the yield condition and the flow rule, are formulated in stress space in terms of the variables $\{\boldsymbol{\sigma}, \boldsymbol{q}\}$, where $\boldsymbol{\sigma}$ is the stress tensor which is a function of $(\boldsymbol{\varepsilon}, \boldsymbol{\varepsilon}^{\mathrm{p}})$, and the internal variables $\boldsymbol{q}$ are functions of $(\boldsymbol{\varepsilon}^{\mathrm{p}}, \boldsymbol{\alpha})$. In the following discussion of classical plasticity, we adopt this point of view and formulate the response functions in stress space. Nevertheless, we regard $\{\boldsymbol{\varepsilon}, \boldsymbol{\varepsilon}^{\mathrm{p}}, \boldsymbol{\alpha}\}$ as the independent variables.

The basic assumptions underlying the formulation of phenomenological models of classical plasticity, leading to a set of local evolution equations for the plastic strain $\boldsymbol{\varepsilon}^{\mathrm{p}}$ and the internal variables $\boldsymbol{q}$, can be summarized as follows.

2.1.1 | Additive decomposition of strain tensor

In the small strain theory, it is assumed that the strain tensor $\boldsymbol{\varepsilon}$ can be additively decomposed into an elastic part $\boldsymbol{\varepsilon}^{\mathrm{e}}$ and a plastic part $\boldsymbol{\varepsilon}^{\mathrm{p}}$ according to the relationship

$$\boldsymbol{\varepsilon} = \boldsymbol{\varepsilon}^{\mathrm{e}} + \boldsymbol{\varepsilon}^{\mathrm{p}}, \qquad \varepsilon_{ij} = \varepsilon_{ij}^{\mathrm{e}} + \varepsilon_{ij}^{\mathrm{p}}. \tag{1}$$

Since the strain tensor $\boldsymbol{\varepsilon}$ is regarded as an independent variable and the evolution of the plastic strain tensor $\boldsymbol{\varepsilon}^{\mathrm{p}}$ is defined by the flow rule, the relation (1) should be viewed as a definition of the elastic strain tensor as $\boldsymbol{\varepsilon}^{\mathrm{e}} = \boldsymbol{\varepsilon} - \boldsymbol{\varepsilon}^{\mathrm{p}}$.

2.1.2 | Elastic stress response

The stress tensor $\boldsymbol{\sigma}$ is expressed from (1) as

$$\boldsymbol{\sigma} = \mathbf{C}^{\mathrm{e}} : \left[\boldsymbol{\varepsilon} - \boldsymbol{\varepsilon}^{\mathrm{p}} \right], \tag{2}$$

where $\mathbf{C}^{\mathrm{e}}$ is the tensor of elastic moduli which is assumed constant.

2.1.3 | Elastic domain and yield condition

We define a function $g : \mathbb{S} \times \mathbb{R}^{n_{\mathrm{iv}}} \rightarrow \mathbb{R}$, where $\mathbb{S} \subset \mathbb{L}(\mathbb{R}^n, \mathbb{R}^n)$ is the subspace of symmetric second-order tensors with dimension $n(n+1)/2$, in which $\mathbb{L}$ is the vector space, called the yield criterion and constrain the admissible states $(\boldsymbol{\sigma}, \boldsymbol{q}) \in \mathbb{S} \times \mathbb{R}^{n_{\mathrm{iv}}}$ in stress space to lie in the set $\mathbb{E}_\sigma$ defined as

$$\mathbb{E}_\sigma = \left\{ (\boldsymbol{\sigma}, \boldsymbol{q}) \in \mathbb{S} \times \mathbb{R}^{n_{\mathrm{iv}}} : g(\boldsymbol{\sigma}, \boldsymbol{q}) \leq 0 \right\}.$$

One refers to the interior of $\mathbb{E}_\sigma$, denoted by $\mathrm{int}(\mathbb{E}_\sigma)$ and given by

$$\mathrm{int}(\mathbb{E}_\sigma) = \left\{ (\boldsymbol{\sigma}, \boldsymbol{q}) \in \mathbb{S} \times \mathbb{R}^{n_{\mathrm{iv}}} : g(\boldsymbol{\sigma}, \boldsymbol{q}) < 0 \right\},$$

as the elastic domain; whereas the boundary of $\mathbb{E}_\sigma$, denoted by $\partial \mathbb{E}_\sigma$ and defined as

$$\partial\mathbb{E}_\sigma = \left\{(\boldsymbol{\sigma}, \boldsymbol{q}) \in \mathbb{S} \times \mathbb{R}^{n_{\mathrm{iv}}} : g(\boldsymbol{\sigma}, \boldsymbol{q}) = 0\right\},$$

is called the yield surface. Note that states $(\boldsymbol{\sigma}, \boldsymbol{q})$ outside $\mathbb{E}_\sigma$ are nonadmissible and are ruled out in classical plasticity.

2.1.4 | Flow rule and hardening law

The key notion of irreversibility of plastic flow by the following (nonsmooth) equations of evolution for $(\boldsymbol{\sigma}, \boldsymbol{q})$;

$$\dot{\boldsymbol{\varepsilon}}^{\mathrm{p}} = \gamma \boldsymbol{r}(\boldsymbol{\sigma}, \boldsymbol{q})$$

and

$$\dot{\boldsymbol{q}} = -\gamma \boldsymbol{h}(\boldsymbol{\sigma}, \boldsymbol{q}),$$

which are referred to as the flow rule and hardening law, respectively. Here, $\boldsymbol{r} : \mathbb{S} \times \mathbb{R}^{n_{\mathrm{iv}}} \to \mathbb{S}$ and $\boldsymbol{h} : \mathbb{S} \times \mathbb{R}^{n_{\mathrm{iv}}} \to \mathbb{R}^{n_{\mathrm{iv}}}$ are prescribed functions which define the direction of plastic flow and the type of hardening. The consistency parameter $\gamma \geq 0$ is assumed to obey the following Kuhn–Tucker complementarity conditions:

$$\gamma \geq 0, \quad g(\boldsymbol{\sigma}, \boldsymbol{q}) \leq 0, \quad \text{and} \quad \gamma g(\boldsymbol{\sigma}, \boldsymbol{q}) = 0. \tag{3}$$

In addition to the conditions (3), $\gamma \geq 0$ satisfies the consistency requirement

$$\gamma \dot{g}(\boldsymbol{\sigma}, \boldsymbol{q}) = 0 \quad \text{if } g(\boldsymbol{\sigma}, \boldsymbol{q}) = 0. \tag{4}$$

In the present context, the conditions (3) and (4) indicate the notion of plastic loading and elastic unloading.

2.2 | J_2-flow theory

In metal plasticity, the internal variables are typically represented as $\boldsymbol{q} = \{\alpha, \boldsymbol{\beta}\}$, where α is the equivalent plastic strain which defines isotropic hardening of the von Mises yield surface and $\boldsymbol{\beta}$ denotes the center of the von Mises yield surface in stress deviator space. As an example, a widely used extension of the classical Prandl–Reuss equations of perfect plasticity that incorporates hardening is obtained by considering linear isotropic elastic response, with elasticity tensor,

$$\mathbf{C}^{\mathrm{e}} = \lambda \mathbf{1} \otimes \mathbf{1} + 2\mu \mathbf{I}, \tag{5}$$

where λ and μ are Lamé's constants, and the second-order and the fourth-order symmetric tensors are designated as

$$\mathbf{1} = \delta_{ij} \boldsymbol{e}_i \otimes \boldsymbol{e}_j \quad \text{and} \quad \mathbf{I} = \frac{1}{2}\left[\delta_{ik}\delta_{jl} + \delta_{il}\delta_{jk}\right] \boldsymbol{e}_i \otimes \boldsymbol{e}_j \otimes \boldsymbol{e}_k \otimes \boldsymbol{e}_l,$$

respectively, and the following pressure insensitive, isotropic, Huber–von Mises yield condition

$$g(\boldsymbol{\sigma}, \alpha, \boldsymbol{\beta}) = |\mathrm{dev}[\boldsymbol{\sigma}] - \boldsymbol{\beta}| - \sqrt{\frac{2}{3}} \left[\sigma_{\mathrm{Y}} + K(\alpha)\right] \leq 0, \tag{6}$$

where

$$\mathrm{dev}[\boldsymbol{\sigma}] = \boldsymbol{\sigma} - \frac{1}{3}\mathrm{tr}[\boldsymbol{\sigma}]\mathbf{1},$$

is the deviatoric part of the stress tensor, σ_{Y} is the one-dimensional flow stress, $\boldsymbol{\beta}$ is the back stress satisfying

$$\mathrm{tr}[\boldsymbol{\beta}] = 0, \tag{7}$$

and $K(\alpha)$ is the isotropic hardening function. Note that an induced norm of second-order tensor is denoted by two vertical bars, defined by $|A| = \sqrt{A_{ij}A_{ij}}$, for any A. It is assumed that $\mathrm{tr}[\beta] = 0$ in (7), that is, the back stress is a deviatoric tensor. To arrive at a compact formulation, it proves convenient to define a relative stress ξ as the difference between the stress deviator $s = \mathrm{dev}[\sigma]$ and the back stress β, as follows:

$$\xi = s - \beta. \tag{8}$$

Hence, Huber–von Mises yield condition (6) can be written as

$$g(\xi, \alpha) = |\xi| - \sqrt{\frac{2}{3}} \left[\sigma_Y + K(\alpha) \right] \leq 0. \tag{9}$$

Denoting the unit normal field to the von Mises cylinder as,

$$n = \frac{\xi}{|\xi|},$$

the associative evolution equations can be written as

$$\dot{\varepsilon}^{\mathrm{p}} = \gamma \frac{\partial g}{\partial \sigma} = \gamma n, \tag{10}$$

$$\dot{\beta} = \gamma \frac{2}{3} H' \frac{\partial g}{\partial \beta} = \gamma \frac{2}{3} H' n, \tag{11}$$

$$\dot{\alpha} = \gamma \frac{\partial g}{\partial \alpha} = \gamma \sqrt{\frac{2}{3}}. \tag{12}$$

It should be noted that the relation (10) is known as the Levy–Saint Venant flow rule. In addition, the relation (11) is also known as the Prager–Ziegler kinematic hardening rule, in which $K(\alpha)$ and $H(\alpha)$ are referred to as the isotropic and kinematic hardening functions, respectively, and

$$H' = \frac{\partial H}{\partial \alpha}.$$

Since $|\dot{\varepsilon}^{\mathrm{p}}| = \gamma$, the relation (12) implies that

$$\alpha = \int_0^t \sqrt{\frac{2}{3}} \, |\dot{\varepsilon}^{\mathrm{p}}| \, d\tau,$$

which is in agreement with the usual definition of equivalent plastic strain. Finally, the elastoplastic tangent moduli in plastic loading are obtained as

$$\mathbf{C}^{\mathrm{ep}} = \kappa \mathbf{1} \otimes \mathbf{1} + 2\mu \left[\mathbf{I} - \frac{1}{3} \mathbf{1} \otimes \mathbf{1} - \frac{n \otimes n}{1 + \frac{H'+K'}{3\mu}} \right], \quad \text{for } \gamma > 0, \tag{13}$$

where $\kappa = \lambda + \frac{2}{3}\mu > 0$ is the bulk modulus and

$$K' = \frac{\partial K}{\partial \alpha}.$$

3 | INCREMENTAL FORMULATION FOR ELASTOPLASTIC ANALYSIS WITH BLOCK NEWTON METHOD

In this work, we propose the formulation for elastoplastic problems as a coupled problem to compute the local response at each material point and the deformation of the overall structure. A key technique in the formulation involves that the internal variables for plasticity are condensed out at each material point.

3.1 | Equilibrium equations

The domain of the problem of interest for the overall structure can be described as the whole domain Ω with boundary Γ. In addition, the Dirichlet and Neumann boundaries are represented as Γ_u and Γ_t, respectively.

The governing equations in Ω can be written as

$$\nabla \cdot \boldsymbol{\sigma} + \boldsymbol{b} = \boldsymbol{0} \quad \text{in} \ \ \Omega, \tag{14}$$

$$\boldsymbol{u} = \overline{\boldsymbol{u}} \quad \text{on} \ \ \Gamma_u, \tag{15}$$

$$\boldsymbol{t} = \overline{\boldsymbol{t}} \quad \text{on} \ \ \Gamma_t, \tag{16}$$

where $\boldsymbol{u}$ denotes the displacement vector, $\boldsymbol{\sigma}$ is the stress tensor calculated from the displacement field $\boldsymbol{u}$, and $\boldsymbol{b}$ and $\boldsymbol{t}$ are the body force per unit volume and the surface traction vector, respectively. In addition, the prescribed displacement and traction vectors are expressed as $\overline{\boldsymbol{u}}$ and $\overline{\boldsymbol{t}}$, respectively. For the purpose of solving the equilibrium equation (14), the Dirichlet boundary condition (15) and the Neumann boundary condition (16) are imposed. Note that, from the balance of angular momentum, the symmetry of the stress tensor $\boldsymbol{\sigma}$ can be implied.

3.2 | Discretization of integration of stress

To avoid dependency of the numerical solutions on convergence paths, the total increments from the previous converged state to the tentative state in the iteration are introduced and the Newton–Raphson algorithm is applied to solve the quasi-static problem. The total strain tensor $\boldsymbol{\varepsilon}_{n+1}$ and the consistency parameter γ_{n+1} at time t_{n+1} can be represented as

$$\boldsymbol{\varepsilon}_{n+1}^{(i+1)} = \boldsymbol{\varepsilon}_n + \Delta\boldsymbol{\varepsilon}^{(i+1)}, \qquad \gamma_{n+1}^{(i+1)} = \gamma_n + \Delta\gamma^{(i+1)},$$

where $\boldsymbol{\varepsilon}_n$ and γ_n are the total strain tensor and the consistency parameter at the previous equilibrium state (at time t_n), respectively, and $\Delta\boldsymbol{\varepsilon}^{(i+1)}$ and $\Delta\gamma^{(i+1)}$ are the total increments from the previous equilibrium state at time t_n to the current $(i+1)$th iteration in the Newton–Raphson algorithm, respectively. In the Newton–Raphson algorithm, the increments $(\Delta\boldsymbol{\varepsilon}$ and $\Delta\gamma)$ at $(i+1)$th iteration can be written as the sum of the increments up to the previous ith iteration and the corrections $(\delta\boldsymbol{\varepsilon}$ and $\delta\gamma)$ by the current $(i+1)$th iteration, as follows:

$$\Delta\boldsymbol{\varepsilon}^{(i+1)} = \Delta\boldsymbol{\varepsilon}^{(i)} + \delta\boldsymbol{\varepsilon}^{(i+1)}, \qquad \Delta\gamma^{(i+1)} = \Delta\gamma^{(i)} + \delta\gamma^{(i+1)}, \tag{17}$$

respectively. Here, the superscript in parentheses denotes the number of iteration, while the subscript describes the time step.

The stress tensor $\boldsymbol{\sigma}$ at the previous equilibrium state can be represented using (2) as

$$\boldsymbol{\sigma}(\boldsymbol{\varepsilon}_n, \gamma_n) = \mathbf{C}^e : \left[\boldsymbol{\varepsilon}_n - \boldsymbol{\varepsilon}^p(\boldsymbol{\varepsilon}_n, \gamma_n) \right],$$

where $\mathbf{C}^e$ is the elasticity tensor, which is assumed to be constant during the deformation. Hence, the incremental form of the stress tensor at time t_{n+1} can be expressed as

$$\boldsymbol{\sigma}(\boldsymbol{\varepsilon}_{n+1}^{(i+1)}, \gamma_{n+1}^{(i+1)}) = \mathbf{C}^e : \left[\boldsymbol{\varepsilon}_{n+1}^{(i+1)} - \boldsymbol{\varepsilon}^p(\boldsymbol{\varepsilon}_{n+1}^{(i+1)}, \gamma_{n+1}^{(i+1)}) \right]. \tag{18}$$

The plastic strain tensor $\boldsymbol{\varepsilon}^p$ can be denoted using an implicit backward difference scheme (A2) as

$$\boldsymbol{\varepsilon}^p(\boldsymbol{\varepsilon}_{n+1}^{(i+1)}, \gamma_{n+1}^{(i+1)}) = \boldsymbol{\varepsilon}^p(\boldsymbol{\varepsilon}_n, \gamma_n) + \{\Delta\gamma^{(i)} + \delta\gamma^{(i+1)}\}\boldsymbol{n}(\boldsymbol{\varepsilon}_{n+1}^{(i+1)}, \gamma_{n+1}^{(i+1)}). \tag{19}$$

Here, the unit normal field to the von Mises cylinder can be linearized as

$$\boldsymbol{n}(\boldsymbol{\varepsilon}_{n+1}^{(i+1)}, \gamma_{n+1}^{(i+1)}) = \boldsymbol{n}(\boldsymbol{\varepsilon}_{n+1}^{(i)}, \gamma_{n+1}^{(i)}) + \frac{\partial \boldsymbol{n}(\boldsymbol{\varepsilon}_{n+1}^{(i)}, \gamma_{n+1}^{(i)})}{\partial \boldsymbol{\varepsilon}} : \delta\boldsymbol{\varepsilon}^{(i+1)} + \frac{\partial \boldsymbol{n}(\boldsymbol{\varepsilon}_{n+1}^{(i)}, \gamma_{n+1}^{(i)})}{\partial \gamma} \cdot \delta\gamma^{(i+1)}, \tag{20}$$

where the unit normal field $\boldsymbol{n}$ at the previous ith iteration can be described using the relative stress $\boldsymbol{\xi}$ as

$$\boldsymbol{n}(\varepsilon_{n+1}^{(i)}, \gamma_{n+1}^{(i)}) = \frac{\boldsymbol{\xi}(\varepsilon_{n+1}^{(i)}, \gamma_{n+1}^{(i)})}{\left|\boldsymbol{\xi}(\varepsilon_{n+1}^{(i)}, \gamma_{n+1}^{(i)})\right|}, \tag{21}$$

and the relative stress at the previous ith iteration is expressed using the stress deviator $\boldsymbol{s}$ and the back stress $\boldsymbol{\beta}$ as

$$\boldsymbol{\xi}(\varepsilon_{n+1}^{(i)}, \gamma_{n+1}^{(i)}) = \boldsymbol{s}(\varepsilon_{n+1}^{(i)}, \gamma_{n+1}^{(i)}) - \boldsymbol{\beta}(\varepsilon_{n+1}^{(i)}, \gamma_{n+1}^{(i)}). \tag{22}$$

From the associative flow rules, the stress deviator $\boldsymbol{s}$ can be depicted as

$$\boldsymbol{s}(\varepsilon_{n+1}^{(i)}, \gamma_{n+1}^{(i)}) = \boldsymbol{s}(\varepsilon_n, \gamma_n) + 2\mu \cdot \mathrm{dev}\left[\Delta\varepsilon^{(i)}\right] - 2\mu\Delta\gamma^{(i)}\boldsymbol{n}(\varepsilon_{n+1}^{(i)}, \gamma_{n+1}^{(i)}), \tag{23}$$

and the back stress $\boldsymbol{\beta}$ is represented using (A3) as

$$\boldsymbol{\beta}(\varepsilon_{n+1}^{(i)}, \gamma_{n+1}^{(i)}) = \boldsymbol{\beta}(\varepsilon_n, \gamma_n) + \frac{2}{3}H'\Delta\gamma^{(i)}\boldsymbol{n}(\varepsilon_{n+1}^{(i)}, \gamma_{n+1}^{(i)}). \tag{24}$$

Substituting (23) and (24) into (22), the relative stress at the previous ith iteration can be written as

$$\boldsymbol{\xi}(\varepsilon_{n+1}^{(i)}, \gamma_{n+1}^{(i)}) = \boldsymbol{\xi}^{\mathrm{tr}} - \left(2\mu + \frac{2}{3}H'\right)\Delta\gamma^{(i)}\boldsymbol{n}(\varepsilon_{n+1}^{(i)}, \gamma_{n+1}^{(i)}), \tag{25}$$

where

$$\boldsymbol{\xi}^{\mathrm{tr}} = \boldsymbol{\xi}(\varepsilon_n, \gamma_n) + 2\mu \cdot \mathrm{dev}\left[\Delta\varepsilon^{(i)}\right]. \tag{26}$$

From the definition in (21), the unit normal field $\boldsymbol{n}$ at the previous ith iteration can be rewritten using the trial relative stress $\boldsymbol{\xi}^{\mathrm{tr}}$ in (26) as

$$\boldsymbol{n}(\varepsilon_{n+1}^{(i)}, \gamma_{n+1}^{(i)}) = \frac{\boldsymbol{\xi}^{\mathrm{tr}}}{\left|\boldsymbol{\xi}^{\mathrm{tr}}\right|}. \tag{27}$$

Thus,

$$\frac{\partial\boldsymbol{n}(\varepsilon_{n+1}^{(i)}, \gamma_{n+1}^{(i)})}{\partial\varepsilon} = \frac{\partial\boldsymbol{n}(\varepsilon_{n+1}^{(i)}, \gamma_{n+1}^{(i)})}{\partial\boldsymbol{\xi}^{\mathrm{tr}}} : \frac{\partial\boldsymbol{\xi}^{\mathrm{tr}}}{\partial\varepsilon} = \frac{2\mu}{\left|\boldsymbol{\xi}^{\mathrm{tr}}\right|}\left[\boldsymbol{\mathsf{I}} - \frac{1}{3}\boldsymbol{1} \otimes \boldsymbol{1} - \boldsymbol{n}(\varepsilon_{n+1}^{(i)}, \gamma_{n+1}^{(i)}) \otimes \boldsymbol{n}(\varepsilon_{n+1}^{(i)}, \gamma_{n+1}^{(i)})\right] \tag{28}$$

and

$$\frac{\partial\boldsymbol{n}(\varepsilon_{n+1}^{(i)}, \gamma_{n+1}^{(i)})}{\partial\gamma} = \frac{\partial\boldsymbol{n}(\varepsilon_{n+1}^{(i)}, \gamma_{n+1}^{(i)})}{\partial\boldsymbol{\xi}^{\mathrm{tr}}} : \frac{\partial\boldsymbol{\xi}^{\mathrm{tr}}}{\partial\gamma} = \boldsymbol{0}, \tag{29}$$

where the unit normal field $\boldsymbol{n}$ has the following property using the relations of $\mathrm{tr}[\boldsymbol{s}] = 0$ and (7) as

$$\mathrm{tr}[\boldsymbol{n}] = \boldsymbol{n} : \boldsymbol{1} = 0. \tag{30}$$

Substituting (28) and (29) into (20), the linearized unit normal field can be expressed as

$$\boldsymbol{n}(\varepsilon_{n+1}^{(i+1)}, \gamma_{n+1}^{(i+1)}) = \boldsymbol{n}(\varepsilon_{n+1}^{(i)}, \gamma_{n+1}^{(i)}) + \frac{2\mu}{\left|\boldsymbol{\xi}^{\mathrm{tr}}\right|}\left[\boldsymbol{\mathsf{I}} - \frac{1}{3}\boldsymbol{1} \otimes \boldsymbol{1} - \boldsymbol{n}(\varepsilon_{n+1}^{(i)}, \gamma_{n+1}^{(i)}) \otimes \boldsymbol{n}(\varepsilon_{n+1}^{(i)}, \gamma_{n+1}^{(i)})\right] : \delta\varepsilon^{(i+1)}. \tag{31}$$

Hence, the plastic strain tensor ε^{p} in (19) can be represented using the linearized unit normal field (31) as

$$\varepsilon^{\mathrm{p}}(\varepsilon_{n+1}^{(i+1)}, \gamma_{n+1}^{(i+1)}) = \varepsilon^{\mathrm{p}}(\varepsilon_{n+1}^{(i)}, \gamma_{n+1}^{(i)}) + \delta\gamma^{(i+1)}\boldsymbol{n}(\varepsilon_{n+1}^{(i)}, \gamma_{n+1}^{(i)}) + \frac{2\mu\Delta\gamma^{(i)}}{\left|\boldsymbol{\xi}^{\mathrm{tr}}\right|}\left[\boldsymbol{\mathsf{I}} - \frac{1}{3}\boldsymbol{1} \otimes \boldsymbol{1} - \boldsymbol{n}(\varepsilon_{n+1}^{(i)}, \gamma_{n+1}^{(i)}) \otimes \boldsymbol{n}(\varepsilon_{n+1}^{(i)}, \gamma_{n+1}^{(i)})\right] : \delta\varepsilon^{(i+1)}, \tag{32}$$

where $\varepsilon^{\mathrm{p}}(\varepsilon_{n+1}^{(i)}, \gamma_{n+1}^{(i)})$ is the plastic strain tensor calculated at the previous ith iteration. Substituting (32) into (18), the stress tensor is linearized as follows:

$$\boldsymbol{\sigma}(\varepsilon_{n+1}^{(i+1)}, \gamma_{n+1}^{(i+1)}) = \boldsymbol{\sigma}(\varepsilon_{n+1}^{(i)}, \gamma_{n+1}^{(i)}) + \left[\mathbf{C}^{\mathrm{e}} - \mathbf{C}^{\mathrm{e}} : \left\{ \frac{2\mu\Delta\gamma^{(i)}}{|\boldsymbol{\xi}^{\mathrm{tr}}|} \left[\mathbf{I} - \frac{1}{3}\mathbf{1}\otimes\mathbf{1} - \boldsymbol{n}(\varepsilon_{n+1}^{(i)}, \gamma_{n+1}^{(i)}) \otimes \boldsymbol{n}(\varepsilon_{n+1}^{(i)}, \gamma_{n+1}^{(i)}) \right] \right\} \right] : \delta\varepsilon^{(i+1)}$$
$$- \left[\mathbf{C}^{\mathrm{e}} : \boldsymbol{n}(\varepsilon_{n+1}^{(i)}, \gamma_{n+1}^{(i)}) \right] \delta\gamma^{(i+1)}, \tag{33}$$

where the stress tensor at the previous ith iteration can be expressed as

$$\boldsymbol{\sigma}(\varepsilon_{n+1}^{(i)}, \gamma_{n+1}^{(i)}) = \mathbf{C}^{\mathrm{e}} : \left[\varepsilon_{n+1}^{(i)} - \varepsilon^{\mathrm{p}}(\varepsilon_{n+1}^{(i)}, \gamma_{n+1}^{(i)}) \right].$$

3.3 | Incremental form of yield condition

The yield condition (6) at time t_n can be described using the relative stress $\boldsymbol{\xi}$ in (8) as the relation (9), and written as the following scalar equation:

$$g(\varepsilon_n, \gamma_n) = |\boldsymbol{\xi}(\varepsilon_n, \gamma_n)| - \sqrt{\frac{2}{3}} \left[\sigma_{\mathrm{Y}} + K(\gamma_n) \right],$$

where the relative stress at the previous equilibrium state is expressed using the stress deviator $\boldsymbol{s}$ and the back stress $\boldsymbol{\beta}$ as

$$\boldsymbol{\xi}(\varepsilon_n, \gamma_n) = \boldsymbol{s}(\varepsilon_n, \gamma_n) - \boldsymbol{\beta}(\varepsilon_n, \gamma_n).$$

From the associative flow rules, the stress deviator $\boldsymbol{s}$ at time t_{n+1} can be depicted as

$$\boldsymbol{s}(\varepsilon_{n+1}^{(i+1)}, \gamma_{n+1}^{(i+1)}) = \boldsymbol{s}(\varepsilon_n, \gamma_n) + 2\mu \cdot \mathrm{dev}\left[\Delta\varepsilon^{(i)} + \delta\varepsilon^{(i+1)} \right] - 2\mu\{\Delta\gamma^{(i)} + \delta\gamma^{(i+1)}\}\boldsymbol{n}(\varepsilon_{n+1}^{(i+1)}, \gamma_{n+1}^{(i+1)}), \tag{34}$$

and the back stress $\boldsymbol{\beta}$ is represented using (A3) as

$$\boldsymbol{\beta}(\varepsilon_{n+1}^{(i+1)}, \gamma_{n+1}^{(i+1)}) = \boldsymbol{\beta}(\varepsilon_n, \gamma_n) + \frac{2}{3}H'\{\Delta\gamma^{(i)} + \delta\gamma^{(i+1)}\}\boldsymbol{n}(\varepsilon_{n+1}^{(i+1)}, \gamma_{n+1}^{(i+1)}). \tag{35}$$

Hence, the relative stress $\boldsymbol{\xi}$ at time t_{n+1} can be written using (34) and (35) as

$$\boldsymbol{\xi}(\varepsilon_{n+1}^{(i+1)}, \gamma_{n+1}^{(i+1)}) = \boldsymbol{\xi}(\varepsilon_n, \gamma_n) + 2\mu \cdot \mathrm{dev}\left[\Delta\varepsilon^{(i)} + \delta\varepsilon^{(i+1)} \right] - \left(2\mu + \frac{2}{3}H' \right) \{\Delta\gamma^{(i)} + \delta\gamma^{(i+1)}\}\boldsymbol{n}(\varepsilon_{n+1}^{(i+1)}, \gamma_{n+1}^{(i+1)}). \tag{36}$$

On the other hand, the norm of the relative stress $|\boldsymbol{\xi}|$ at time t_{n+1} is a function of the parameter h and first-order (Taylor's) expansion about $h = 0$ gives

$$\left| \boldsymbol{\xi}(\varepsilon_{n+1}^{(i+1)}, \gamma_{n+1}^{(i+1)}) \right| = \left| \boldsymbol{\xi}(\varepsilon_{n+1}^{(i)}, \gamma_{n+1}^{(i)}) \right| + \frac{d}{dh}\Big|_{h=0} \left| \boldsymbol{\xi}(\varepsilon_{n+1}^{(i)} + h\delta\varepsilon^{(i+1)}, \gamma_{n+1}^{(i)} + h\delta\gamma^{(i+1)}) \right|. \tag{37}$$

Similarly to the linearized form of the unit normal field (20), first-order (Taylor's) expansion for the unit normal field $\boldsymbol{n}$ at the previous ith iteration yields

$$\boldsymbol{n}(\varepsilon_{n+1}^{(i)} + h\delta\varepsilon^{(i+1)}, \gamma_{n+1}^{(i)} + h\delta\gamma^{(i+1)}) = \boldsymbol{n}(\varepsilon_{n+1}^{(i)}, \gamma_{n+1}^{(i)}) + \frac{\partial\boldsymbol{n}(\varepsilon_{n+1}^{(i)}, \gamma_{n+1}^{(i)})}{\partial\varepsilon} : h\delta\varepsilon^{(i+1)} + \frac{\partial\boldsymbol{n}(\varepsilon_{n+1}^{(i)}, \gamma_{n+1}^{(i)})}{\partial\gamma} \cdot h\delta\gamma^{(i+1)} + \mathcal{O}(h^2);$$

hence, it is rewritten by substituting (28) and (29) as

$$\boldsymbol{n}(\varepsilon_{n+1}^{(i)} + h\delta\varepsilon^{(i+1)}, \gamma_{n+1}^{(i)} + h\delta\gamma^{(i+1)}) = \boldsymbol{n}(\varepsilon_{n+1}^{(i)}, \gamma_{n+1}^{(i)})$$
$$+ \frac{2\mu}{|\boldsymbol{\xi}^{\mathrm{tr}}|} \left[\mathbf{I} - \frac{1}{3}\mathbf{1}\otimes\mathbf{1} - \boldsymbol{n}(\varepsilon_{n+1}^{(i)}, \gamma_{n+1}^{(i)}) \otimes \boldsymbol{n}(\varepsilon_{n+1}^{(i)}, \gamma_{n+1}^{(i)}) \right] : h\delta\varepsilon^{(i+1)} + \mathcal{O}(h^2). \tag{38}$$

Thus, the second term of (37) is described using (36) and (38) and written after some manipulations as

$$\frac{d}{dh}\Big|_{h=0} \Big| \xi(\varepsilon_{n+1}^{(i)} + h\delta\varepsilon^{(i+1)}, \gamma_{n+1}^{(i)} + h\delta\gamma^{(i+1)}) \Big| = 2\mu \boldsymbol{n}(\varepsilon_{n+1}^{(i)}, \gamma_{n+1}^{(i)}) : \text{dev}\big[\delta\varepsilon^{(i+1)}\big] - \left(2\mu + \frac{2}{3}H'\right)\delta\gamma^{(i+1)}. \tag{39}$$

Substituting (39) into (37), the linearized form of the norm of the relative stress $|\xi|$ at time t_{n+1} can be denoted as

$$\Big| \xi(\varepsilon_{n+1}^{(i+1)}, \gamma_{n+1}^{(i+1)}) \Big| = \Big| \xi(\varepsilon_{n+1}^{(i)}, \gamma_{n+1}^{(i)}) \Big| + 2\mu \boldsymbol{n}(\varepsilon_{n+1}^{(i)}, \gamma_{n+1}^{(i)}) : \text{dev}\big[\delta\varepsilon^{(i+1)}\big] - \left(2\mu + \frac{2}{3}H'\right)\delta\gamma^{(i+1)}.$$

Here, the inner product between the unit normal field $\boldsymbol{n}$ and the strain deviator $\text{dev}[\varepsilon]$ can be represented as

$$\boldsymbol{n} : \text{dev}[\varepsilon] = \boldsymbol{n} : \text{dev}[\varepsilon] + \boldsymbol{n} : \frac{1}{3}\text{tr}[\varepsilon]\mathbf{1} = \boldsymbol{n} : \varepsilon,$$

where the property of the unit normal field $\boldsymbol{n}$ in (30) is employed. Hence, the linearized form of the norm of the relative stress $|\xi|$ at time t_{n+1} can be written as

$$\Big| \xi(\varepsilon_{n+1}^{(i+1)}, \gamma_{n+1}^{(i+1)}) \Big| = \Big| \xi(\varepsilon_{n+1}^{(i)}, \gamma_{n+1}^{(i)}) \Big| + 2\mu \boldsymbol{n}(\varepsilon_{n+1}^{(i)}, \gamma_{n+1}^{(i)}) : \delta\varepsilon^{(i+1)} - \left(2\mu + \frac{2}{3}H'\right)\delta\gamma^{(i+1)}. \tag{40}$$

On the other hand, the incremental form of the isotropic hardening function can be expressed using the relation (A4) as follows:

$$K(\gamma_{n+1}^{(i+1)}) = K(\gamma_{n+1}^{(i)}) + \sqrt{\frac{2}{3}}K'(\gamma_{n+1}^{(i)})\delta\gamma^{(i+1)}. \tag{41}$$

From (40) and (41), the incremental form of the yield condition at time t_{n+1} can be obtained as follows:

$$g(\varepsilon_{n+1}^{(i+1)}, \gamma_{n+1}^{(i+1)}) = g(\varepsilon_{n+1}^{(i)}, \gamma_{n+1}^{(i)}) + 2\mu \boldsymbol{n}(\varepsilon_{n+1}^{(i)}, \gamma_{n+1}^{(i)}) : \delta\varepsilon^{(i+1)} - \left\{2\mu + \frac{2}{3}\left[H' + K'(\gamma_{n+1}^{(i)})\right]\right\}\delta\gamma^{(i+1)}. \tag{42}$$

Remark 1. In the proposed approach, when the yield surface, which multiple unit normal fields can be defined (e.g., the Tresca yield surface or the Mohr–Coulomb yield surface), is employed, it will be required to formulate with conditional bifurcation,[47] similarly to the conventional return mapping algorithm.

3.4 | Coupled problem at material point

From the small strain theory, the strain tensor ε can be described using only the displacement vector $\boldsymbol{u}$ as

$$\varepsilon(\boldsymbol{u}) = \frac{1}{2}\left\{ \frac{\partial \boldsymbol{u}}{\partial \boldsymbol{x}} + \left(\frac{\partial \boldsymbol{u}}{\partial \boldsymbol{x}}\right)^{\mathrm{T}} \right\},$$

where the superscript T denotes the transpose. For the application to the finite element method based on the conventional displacement method, the unknowns of the displacement field can be represented as

$$\boldsymbol{u}_{n+1}^{(i+1)} = \boldsymbol{u}_n + \Delta\boldsymbol{u}^{(i+1)}, \quad \Delta\boldsymbol{u}^{(i+1)} = \Delta\boldsymbol{u}^{(i)} + \delta\boldsymbol{u}^{(i+1)},$$

where $\boldsymbol{u}_n$ is the total displacement vector at the previous equilibrium state (at time t_n), $\Delta\boldsymbol{u}^{(i+1)}$ is the total increment from the previous equilibrium state at time t_n to the current $(i+1)$th iteration in the Newton–Raphson algorithm, and $\delta\boldsymbol{u}^{(i+1)}$ denotes the correction from the sum of the increments up to the previous ith iteration $\Delta\boldsymbol{u}^{(i)}$. Hence, the strain tensors can be expressed as follows:

$$\varepsilon_n = \varepsilon(\boldsymbol{u}_n), \quad \Delta\varepsilon^{(i)} = \varepsilon(\Delta\boldsymbol{u}^{(i)}), \quad \delta\varepsilon^{(i+1)} = \varepsilon(\delta\boldsymbol{u}^{(i+1)}), \quad \varepsilon_{n+1}^{(i+1)} = \varepsilon(\boldsymbol{u}_{n+1}^{(i+1)}) = \varepsilon(\boldsymbol{u}_n + \Delta\boldsymbol{u}^{(i)} + \delta\boldsymbol{u}^{(i+1)}).$$

In the situation of the evolution of the plasticity during the deformation subjected to an external force $\boldsymbol{f}$ per unit volume, we set the following problem:

Find the displacement field $\boldsymbol{u}$ and the consistency parameter γ such that

$$\boldsymbol{\nabla} \cdot \boldsymbol{\sigma}(\boldsymbol{u}, \gamma) = \boldsymbol{f} \qquad \text{in } \Omega, \tag{43}$$

$$g(\boldsymbol{u}, \gamma) = |\boldsymbol{\xi}(\boldsymbol{u}, \gamma)| - \sqrt{\frac{2}{3}} [\sigma_Y + K(\gamma)] = 0 \quad \text{in } \Omega. \tag{44}$$

When the above two equations (43) and (44) are discretized and expressed in the form of an increment to be solved by Newton method, the following problem can be obtained by rewriting the two equations (33) and (42) with the displacement field $\boldsymbol{u}$ and the internal variables for plasticity:

Find corrections for the displacement field $\delta\boldsymbol{u}^{(i+1)}$ and the consistency parameter $\delta\gamma^{(i+1)}$ such that

$$\boldsymbol{\nabla} \cdot \{\mathbf{C} : \boldsymbol{\varepsilon}(\delta\boldsymbol{u}^{(i+1)}) + \boldsymbol{L}\delta\gamma^{(i+1)}\} = \boldsymbol{f}_{n+1} - \boldsymbol{\nabla} \cdot \boldsymbol{\sigma}(\boldsymbol{u}_{n+1}^{(i)}, \gamma_{n+1}^{(i)}) \qquad \text{in } \Omega, \tag{45}$$

$$\boldsymbol{M} : \boldsymbol{\varepsilon}(\delta\boldsymbol{u}^{(i+1)}) + N\delta\gamma^{(i+1)} = -g(\boldsymbol{u}_{n+1}^{(i)}, \gamma_{n+1}^{(i)}) \qquad \text{in } \Omega, \tag{46}$$

where

$$\mathbf{C} = \mathbf{C}^e - \mathbf{C}^e : \left\{ \frac{2\mu\Delta\gamma^{(i)}}{|\boldsymbol{\xi}^{\text{tr}}|} \left[\mathbf{I} - \frac{1}{3}\mathbf{1} \otimes \mathbf{1} - \boldsymbol{n}(\boldsymbol{u}_{n+1}^{(i)}, \gamma_{n+1}^{(i)}) \otimes \boldsymbol{n}(\boldsymbol{u}_{n+1}^{(i)}, \gamma_{n+1}^{(i)}) \right] \right\}, \tag{47}$$

$$\boldsymbol{L} = -\mathbf{C}^e : \boldsymbol{n}(\boldsymbol{u}_{n+1}^{(i)}, \gamma_{n+1}^{(i)}) = -2\mu\boldsymbol{n}(\boldsymbol{u}_{n+1}^{(i)}, \gamma_{n+1}^{(i)}), \tag{48}$$

$$\boldsymbol{M} = 2\mu\boldsymbol{n}(\boldsymbol{u}_{n+1}^{(i)}, \gamma_{n+1}^{(i)}), \tag{49}$$

$$N = -\left\{ 2\mu + \frac{2}{3}\left[H' + K'(\gamma_{n+1}^{(i)}) \right] \right\}. \tag{50}$$

In general, the internal variables for plasticity are independent with the displacement field. By virtue of this idea, static condensation can be applied to the formulations at material point. Thus, the internal variables for plasticity can be condensed out of the equilibrium equation (45). From (46), the correction of the consistency parameter $\delta\gamma^{(i+1)}$ is expressed as

$$\delta\gamma^{(i+1)} = -N^{-1}\boldsymbol{M} : \boldsymbol{\varepsilon}(\delta\boldsymbol{u}^{(i+1)}) - N^{-1} \cdot g(\boldsymbol{u}_{n+1}^{(i)}, \gamma_{n+1}^{(i)}). \tag{51}$$

Since the correction of the consistency parameter $\delta\gamma^{(i+1)}$ is calculated using (51), it can be a positive or negative value. Hence, the total increment of the consistency parameter $\Delta\gamma^{(i+1)}$, which is computed using (17), may be a negative value during the iteration in the Newton–Raphson algorithm. However, it is not allowed that the consistency parameter γ becomes negative according to the Kuhn–Tucker complementarity conditions (3), and the consistency parameter γ should not be recovered even if the situation of the unloading. Thus, the total increment of the consistency parameter $\Delta\gamma^{(i+1)}$ should be not negative. Therefore, if the total increment of the consistency parameter $\Delta\gamma^{(i+1)}$ is calculated as negative in the iterative calculation, the value should be replaced by zero, that is, $\Delta\gamma^{(i+1)} \equiv 0$. It should be noted that the above operation is synonymous with the fact that the evolution of the plasticity does not occur within the time step $[t_n, t_{n+1}]$.

Substituting (51) into (45) and arranging the known and the unknown terms, the incremental form of the equilibrium equation can be represented as

$$\boldsymbol{\nabla} \cdot \left\{ \left[\mathbf{C} - N^{-1} \boldsymbol{L} \otimes \boldsymbol{M} \right] : \varepsilon(\delta \boldsymbol{u}^{(i+1)}) \right\} = \boldsymbol{f}_{n+1} - \boldsymbol{\nabla} \cdot \sigma(\boldsymbol{u}_{n+1}^{(i)}, \gamma_{n+1}^{(i)}) - \boldsymbol{\nabla} \cdot \left[- \left\{ N^{-1} \cdot g(\boldsymbol{u}_{n+1}^{(i)}, \gamma_{n+1}^{(i)}) \right\} \boldsymbol{L} \right] \quad \text{in } \Omega. \tag{52}$$

Here, the stress corrector σ_{g}, whose role is to correct the stress state to be on the yield surface, can be defined using the residual for the yield condition as

$$\sigma_{\mathrm{g}}(\boldsymbol{u}_{n+1}^{(i)}, \gamma_{n+1}^{(i)}) = - \left\{ N^{-1} \cdot g(\boldsymbol{u}_{n+1}^{(i)}, \gamma_{n+1}^{(i)}) \right\} \boldsymbol{L}. \tag{53}$$

Note that, within the proposed approach, the tangent moduli $\mathbf{C}^{\mathrm{ep}}$ can be expressed in a concrete form as

$$\mathbf{C}^{\mathrm{ep}}(\boldsymbol{u}_{n+1}^{(i)}, \gamma_{n+1}^{(i)}) = \mathbf{C} - N^{-1} \boldsymbol{L} \otimes \boldsymbol{M}$$
$$= \kappa \mathbf{1} \otimes \mathbf{1} + 2\mu \left\{ 1 - \frac{2\mu \Delta \gamma^{(i)}}{|\xi^{\mathrm{tr}}|} \right\} \left[\mathsf{I} - \frac{1}{3} \mathbf{1} \otimes \mathbf{1} \right]$$
$$- 2\mu \left\{ \frac{1}{1 + \frac{1}{3\mu} \left[H' + K'(\gamma_{n+1}^{(i)}) \right]} - \frac{2\mu \Delta \gamma^{(i)}}{|\xi^{\mathrm{tr}}|} \right\} \boldsymbol{n}(\boldsymbol{u}_{n+1}^{(i)}, \gamma_{n+1}^{(i)}) \otimes \boldsymbol{n}(\boldsymbol{u}_{n+1}^{(i)}, \gamma_{n+1}^{(i)}). \tag{54}$$

By deriving analytically as in (54), it is shown that the tangent moduli become a similar form of the algorithmic tangent moduli (A11) in the conventional return mapping algorithm. It should be noted that, in the proposed approach, the tangent moduli can be constructed algebraically from the incremental forms (45) and (46), and it is not necessary to derive the analytical form like (54). Thus, the incremental form of the equilibrium equation (52) can be rewritten using the tangent moduli (54) and the stress corrector (53) as

$$\boldsymbol{\nabla} \cdot \left\{ \mathbf{C}^{\mathrm{ep}}(\boldsymbol{u}_{n+1}^{(i)}, \gamma_{n+1}^{(i)}) : \varepsilon(\delta \boldsymbol{u}^{(i+1)}) \right\} = \boldsymbol{f}_{n+1} - \boldsymbol{\nabla} \cdot \sigma(\boldsymbol{u}_{n+1}^{(i)}, \gamma_{n+1}^{(i)}) - \boldsymbol{\nabla} \cdot \sigma_{\mathrm{g}}(\boldsymbol{u}_{n+1}^{(i)}, \gamma_{n+1}^{(i)}) \quad \text{in } \Omega. \tag{55}$$

In the proposed approach, since the global iterative calculation can be performed to simultaneously satisfy the equilibrium equation and the yield condition, the temporary stress state obtained during the global iterative calculation is allowed to be outside of $\mathbb{E}_\sigma$ (refer Section 2.1.3). However, since the proposed formulation does not depend on the numerical solutions on convergence paths, the convergence is finally judged when the stress state exists on the yield surface.

Procedures of updating stress state and constructing tangent moduli are summarized in Box 1. Note that, according to the algorithm in Box 1, the values are calculated based solely on the converged values at the beginning of the time step t_n. Hence, the (nonconverged) values at the previous iteration play no explicit role in the stress update. Therefore, the proposed approach avoids dependency of the numerical solutions on convergence paths, similarly to the conventional return mapping algorithm.[45,46] In addition, it should be noted that the tangent moduli for the first calculation from the previous equilibrium state coincide with the "continuum" tangent moduli in (13), similarly to the conventional return mapping algorithm, as described in Box 2.

Box 1 Procedure of stress update for nonlinear isotropic/kinematic hardening

1. Compute trial elastic stress.

$$\mathrm{dev}\left[\varepsilon(\boldsymbol{u}_{n+1}^{(k+1)}) \right] = \varepsilon(\boldsymbol{u}_{n+1}^{(k+1)}) - \frac{1}{3} \left(\mathrm{tr}\left[\varepsilon(\boldsymbol{u}_{n+1}^{(k+1)}) \right] \right) \mathbf{1}$$
$$\boldsymbol{s}^{\mathrm{tr}} = 2\mu \left\{ \mathrm{dev}\left[\varepsilon(\boldsymbol{u}_{n+1}^{(k+1)}) \right] - \varepsilon^{\mathrm{p}}(\boldsymbol{u}_n, \gamma_n) \right\}$$
$$\xi^{\mathrm{tr}} = \boldsymbol{s}^{\mathrm{tr}} - \beta(\boldsymbol{u}_n, \gamma_n)$$
$$\boldsymbol{n}(\boldsymbol{u}_{n+1}^{(k+1)}, \gamma_{n+1}^{(k+1)}) = \frac{\xi^{\mathrm{tr}}}{|\xi^{\mathrm{tr}}|}$$

2. Check consistency parameter $\Delta \gamma^{(k+1)}$.
   IF $\Delta \gamma^{(k+1)} > 0$ THEN:
   2.1. Plastic case.

2.1.1. Update plastic strain, back stress, and stress.

$$\varepsilon^{\mathrm{p}}(\boldsymbol{u}_{n+1}^{(k+1)}, \gamma_{n+1}^{(k+1)}) = \varepsilon^{\mathrm{p}}(\boldsymbol{u}_n, \gamma_n) + \Delta\gamma^{(k+1)}\boldsymbol{n}(\boldsymbol{u}_{n+1}^{(k+1)}, \gamma_{n+1}^{(k+1)})$$

$$\alpha(\gamma_{n+1}^{(k+1)}) = \alpha(\gamma_n) + \sqrt{\frac{2}{3}}\Delta\gamma^{(k+1)}$$

$$\boldsymbol{\beta}(\boldsymbol{u}_{n+1}^{(k+1)}, \gamma_{n+1}^{(k+1)}) = \boldsymbol{\beta}(\boldsymbol{u}_n, \gamma_n) + \sqrt{\frac{2}{3}}\left[H(\alpha(\gamma_{n+1}^{(k+1)})) - H(\alpha(\gamma_n))\right]\boldsymbol{n}(\boldsymbol{u}_{n+1}^{(k+1)}, \gamma_{n+1}^{(k+1)})$$

$$\boldsymbol{\sigma}(\boldsymbol{u}_{n+1}^{(k+1)}, \gamma_{n+1}^{(k+1)}) = \kappa\ \mathrm{tr}\left[\varepsilon(\boldsymbol{u}_{n+1}^{(k+1)})\right] + \boldsymbol{s}^{\mathrm{tr}} - 2\mu\Delta\gamma^{(k+1)}\boldsymbol{n}(\boldsymbol{u}_{n+1}^{(k+1)}, \gamma_{n+1}^{(k+1)})$$

$$\boldsymbol{s}(\boldsymbol{u}_{n+1}^{(k+1)}, \gamma_{n+1}^{(k+1)}) = \boldsymbol{s}^{\mathrm{tr}} - 2\mu\Delta\gamma_{n+1}^{(k+1)}\boldsymbol{n}(\boldsymbol{u}_{n+1}^{(k+1)}, \gamma_{n+1}^{(k+1)})$$

$$\boldsymbol{\xi}(\boldsymbol{u}_{n+1}^{(k+1)}, \gamma_{n+1}^{(k+1)}) = \boldsymbol{s}(\boldsymbol{u}_{n+1}^{(k+1)}, \gamma_{n+1}^{(k+1)}) - \boldsymbol{\beta}(\boldsymbol{u}_{n+1}^{(k+1)}, \gamma_{n+1}^{(k+1)})$$

2.1.2. Compute stress corrector.

$$g(\boldsymbol{u}_{n+1}^{(k+1)}, \gamma_{n+1}^{(k+1)}) = \left|\boldsymbol{\xi}(\boldsymbol{u}_{n+1}^{(k+1)}, \gamma_{n+1}^{(k+1)})\right| - \sqrt{\frac{2}{3}}\left[\sigma_{\mathrm{Y}} + K(\gamma_{n+1}^{(k+1)})\right]$$

$$\boldsymbol{\sigma}_{\mathrm{g}}(\boldsymbol{u}_{n+1}^{(k+1)}, \gamma_{n+1}^{(k+1)}) = -\left\{N^{-1}(\gamma_{n+1}^{(k+1)}) \cdot g(\boldsymbol{u}_{n+1}^{(k+1)}, \gamma_{n+1}^{(k+1)})\right\}\boldsymbol{L}(\boldsymbol{u}_{n+1}^{(k+1)}, \gamma_{n+1}^{(k+1)})$$

ELSE ($\Delta\gamma^{(k+1)} = 0$) :
2.2. Elastic case.

$$\boldsymbol{s}(\boldsymbol{u}_{n+1}^{(k+1)}, \gamma_{n+1}^{(k+1)}) = \boldsymbol{s}^{\mathrm{tr}}$$

$$\boldsymbol{\xi}(\boldsymbol{u}_{n+1}^{(k+1)}, \gamma_{n+1}^{(k+1)}) = \boldsymbol{\xi}^{\mathrm{tr}}$$

2.2.1. Check yield condition.

$$g(\boldsymbol{u}_{n+1}^{(k+1)}, \gamma_{n+1}^{(k+1)}) = \left|\boldsymbol{\xi}(\boldsymbol{u}_{n+1}^{(k+1)}, \gamma_{n+1}^{(k+1)})\right| - \sqrt{\frac{2}{3}}\left[\sigma_{\mathrm{Y}} + K(\gamma_{n+1}^{(k+1)})\right]$$

IF $g(\boldsymbol{u}_{n+1}^{(k+1)}, \gamma_{n+1}^{(k+1)}) > 0$ THEN:

$$\boldsymbol{\sigma}_{\mathrm{g}}(\boldsymbol{u}_{n+1}^{(k+1)}, \gamma_{n+1}^{(k+1)}) = -\left\{N^{-1}(\gamma_{n+1}^{(k+1)}) \cdot g(\boldsymbol{u}_{n+1}^{(k+1)}, \gamma_{n+1}^{(k+1)})\right\}\boldsymbol{L}(\boldsymbol{u}_{n+1}^{(k+1)}, \gamma_{n+1}^{(k+1)})$$

ELSE ($g(\boldsymbol{u}_{n+1}^{(k+1)}, \gamma_{n+1}^{(k+1)}) \leq 0$) :

$$\boldsymbol{n}(\boldsymbol{u}_{n+1}^{(k+1)}, \gamma_{n+1}^{(k+1)}) \equiv \boldsymbol{0}$$

$$g(\boldsymbol{u}_{n+1}^{(k+1)}, \gamma_{n+1}^{(k+1)}) \equiv 0$$

$$\boldsymbol{\sigma}_{\mathrm{g}}(\boldsymbol{u}_{n+1}^{(k+1)}, \gamma_{n+1}^{(k+1)}) \equiv \boldsymbol{0}$$

ENDIF.
ENDIF.
3. Compute tangent moduli.

$$\mathbf{C}^{\mathrm{ep}}(\boldsymbol{u}_{n+1}^{(k+1)}, \gamma_{n+1}^{(k+1)}) = \mathbf{C}(\boldsymbol{u}_{n+1}^{(k+1)}, \gamma_{n+1}^{(k+1)}) - N^{-1}(\gamma_{n+1}^{(k+1)})\boldsymbol{L}(\boldsymbol{u}_{n+1}^{(k+1)}, \gamma_{n+1}^{(k+1)}) \otimes \boldsymbol{M}(\boldsymbol{u}_{n+1}^{(k+1)}, \gamma_{n+1}^{(k+1)})$$

where

$$\mathbf{C}(\boldsymbol{u}_{n+1}^{(k+1)}, \gamma_{n+1}^{(k+1)}) = \mathbf{C}^{\mathrm{e}} - \mathbf{C}^{\mathrm{e}} : \left\{\frac{2\mu\Delta\gamma^{(k+1)}}{|\boldsymbol{\xi}^{\mathrm{tr}}|}\left[\mathbf{I} - \frac{1}{3}\mathbf{1} \otimes \mathbf{1} - \boldsymbol{n}(\boldsymbol{u}_{n+1}^{(k+1)}, \gamma_{n+1}^{(k+1)}) \otimes \boldsymbol{n}(\boldsymbol{u}_{n+1}^{(k+1)}, \gamma_{n+1}^{(k+1)})\right]\right\}$$

$$\boldsymbol{L}(\boldsymbol{u}_{n+1}^{(k+1)}, \gamma_{n+1}^{(k+1)}) = -2\mu\boldsymbol{n}(\boldsymbol{u}_{n+1}^{(k+1)}, \gamma_{n+1}^{(k+1)})$$

$$\boldsymbol{M}(\boldsymbol{u}_{n+1}^{(k+1)}, \gamma_{n+1}^{(k+1)}) = 2\mu\boldsymbol{n}(\boldsymbol{u}_{n+1}^{(k+1)}, \gamma_{n+1}^{(k+1)})$$

$$N(\gamma_{n+1}^{(k+1)}) = -\left\{2\mu + \frac{2}{3}\left[H' + K'(\gamma_{n+1}^{(k+1)})\right]\right\}$$

3.5 | Discretization with finite element method

To solve the equilibrium equations (14), (15), and (16) in the overall structure, we employ the finite element discretization. It should be noted that the equilibrium equation at the material point is defined at the integration point in the discretized element.

3.5.1 | Principle of virtual work

The weak form of the equilibrium equation for the overall structure can be expressed using the admissible displacement field $\boldsymbol{u}$ as

$$G(\boldsymbol{u}; \boldsymbol{v}) = \int_{\Omega} \boldsymbol{\sigma}(\boldsymbol{u}) : \boldsymbol{\varepsilon}(\boldsymbol{v}) \, d\Omega - \int_{\Omega} \boldsymbol{b} \cdot \boldsymbol{v} \, d\Omega - \int_{\Gamma} \bar{\boldsymbol{t}} \cdot \boldsymbol{v} \, d\Gamma = 0,$$

where $\boldsymbol{v}$ is the virtual displacement vector in Ω and $\boldsymbol{\varepsilon}(\boldsymbol{v})$ is the virtual strain tensor calculated using the virtual displacement field $\boldsymbol{v}$. Hence, the weak form of the incremental form for the equilibrium equation (45) can be described as

$$G(\delta\boldsymbol{u}, \delta\gamma; \delta\boldsymbol{v}) = \int_{\Omega} \boldsymbol{\sigma}(\boldsymbol{u}_{n+1}^{(i)}, \gamma_{n+1}^{(i)}) : \boldsymbol{\varepsilon}(\delta\boldsymbol{v}) \, d\Omega + \int_{\Omega} \left\{ \mathbf{C} : \boldsymbol{\varepsilon}(\delta\boldsymbol{u}^{(i+1)}) + L\delta\gamma^{(i+1)} \right\} : \boldsymbol{\varepsilon}(\delta\boldsymbol{v}) \, d\Omega - \int_{\Omega} \boldsymbol{f}_{n+1} \cdot \delta\boldsymbol{v} \, d\Omega = 0.$$

Thus, the incremental form of the problem to be solved in the situation of the evolution of the plasticity during the deformation can be rewritten as follows:

Find corrections for the displacement field $\delta\boldsymbol{u}^{(i+1)}$ and the consistency parameter $\delta\gamma^{(i+1)}$ such that for any admissible variable $\delta\boldsymbol{v}$ it holds that

$$\int_{\Omega} \left\{ \mathbf{C} : \boldsymbol{\varepsilon}(\delta\boldsymbol{u}^{(i+1)}) \right\} : \boldsymbol{\varepsilon}(\delta\boldsymbol{v}) \, d\Omega + \int_{\Omega} \left\{ L\delta\gamma^{(i+1)} \right\} : \boldsymbol{\varepsilon}(\delta\boldsymbol{v}) \, d\Omega = \int_{\Omega} \boldsymbol{f}_{n+1} \cdot \delta\boldsymbol{v} \, d\Omega - \int_{\Omega} \boldsymbol{\sigma}(\boldsymbol{u}_{n+1}^{(i)}, \gamma_{n+1}^{(i)}) : \boldsymbol{\varepsilon}(\delta\boldsymbol{v}) \, d\Omega, \quad (56)$$

$$\boldsymbol{M} : \boldsymbol{\varepsilon}(\delta\boldsymbol{u}^{(i+1)}) + N\delta\gamma^{(i+1)} = -g(\boldsymbol{u}_{n+1}^{(i)}, \gamma_{n+1}^{(i)}) \qquad \text{in } \Omega. \quad (57)$$

3.5.2 | Incremental form of discretized variational equations

In this work, we employ the finite element discretization to solve the equilibrium equation for the overall structure. The global discretized equation of the incremental form for the coupled problem in (56) and (57) can be expressed using the global stiffness matrices $\mathbf{K}_{UU}$, $\mathbf{K}_{UQ}$, $\mathbf{K}_{QU}$, and $\mathbf{K}_{QQ}$, the global displacement vector $\mathbf{U}$, the global vector form of internal variables $\mathbf{Q}$, which is constructed by the consistency parameter only, the residual force vector $\mathbf{R}_f$, and the global residual vector $\mathbf{R}_g$, whose subvectors are represented by $\mathbf{r}_g$, in the following abstract partitioned form as

$$\begin{bmatrix} \mathbf{K}_{UU} & \mathbf{K}_{UQ} \\ \mathbf{K}_{QU} & \mathbf{K}_{QQ} \end{bmatrix} \begin{Bmatrix} \mathbf{U} \\ \mathbf{Q} \end{Bmatrix} = \begin{Bmatrix} \mathbf{R}_f \\ \mathbf{R}_g \end{Bmatrix}, \quad (58)$$

where

$$\mathbf{R}_f = \overset{n_{el}}{\underset{e=1}{\mathbf{A}}} (\mathbf{r}_f), \quad (59)$$

$$\mathbf{R}_g = \left[\mathbf{r}_g \right]. \quad (60)$$

Here, n_{el} is the number of element, $\mathbf{A}$ denotes the conventional assembly operator, and the subvector $\mathbf{r}_g$ is the residual vector for the yield condition, which has n_{gi} components, where n_{gi} is the number of the Gauss integration point in an element. The global discretized equation (58) has the same form as that derived from the monolithic schemes[31,32] using the linearization of the equilibrium equation and the algebraic equation. The one-level method presented by Ecker et al.[32] corresponds to the method to solve the global discretized equation (58), which the internal variables $\mathbf{Q}$ are left as the global degrees of freedom. On the other hand, Ellsiepen and Hartmann[31] computes the global displacement vector $\mathbf{U}$ after determining the internal variables $\mathbf{Q}$ by local iterative calculation for satisfying the algebraic equation. In this study, on the basis of the coupled problem at material point (refer Section 3.4) and the incremental form of the equilibrium equation (55), the procedure based on the block Newton method to solve the global discretized equation (58) is shown below. Note that the proposed approach can be implemented as well as the conventional displacement method without local iterative calculation, and the tangent stiffness matrix is kept of the advantage of a band-structured sparse matrix.

In the proposed approach, the consistency parameter can be eliminated on the element level, since the consistency parameter is independent with the displacement vector. By virtue of this feature, the number of unknowns in the resulting linear system of equations for the proposed approach is same as that for the conventional displacement method. Hence, the global discretized equation in the matrix form of the incremental form for the equilibrium equation can be described using the global stiffness matrix $\mathbf{K}$, the global displacement vector $\mathbf{U}$, and the global residual force vector $\mathbf{R}$ and assembling element arrays as

$$\mathbf{KU} = \mathbf{R}, \tag{61}$$

where

$$\mathbf{K} = \mathop{\mathbf{A}}_{e=1}^{n_{el}} (\mathbf{k}), \tag{62}$$

$$\mathbf{R} = \mathop{\mathbf{A}}_{e=1}^{n_{el}} (\mathbf{r}). \tag{63}$$

In the region Ω_e in an element, the element stiffness matrix $\mathbf{k}$ and the element residual force vector $\mathbf{r}$ can be expressed as

$$\mathbf{k} = \mathbf{k}_{uu} - \mathbf{k}_{uq}\mathbf{k}_{qq}^{-1}\mathbf{k}_{qu}, \tag{64}$$

$$\mathbf{r} = \mathbf{r}_f - \mathbf{k}_{uq}\mathbf{k}_{qq}^{-1}\mathbf{r}_g, \tag{65}$$

where

$$\mathbf{k}_{uu} = \int_{\Omega_e} \mathbf{B}^{\mathrm{T}}\mathbf{D}\mathbf{B} \, d\Omega = \sum_{j=1}^{n_{gi}} w_{<j>}\mathbf{B}_{<j>}^{\mathrm{T}}\mathbf{D}_{<j>}\mathbf{B}_{<j>}, \tag{66}$$

$$\mathbf{k}_{uq} = \int_{\Omega_e} \mathbf{B}^{\mathrm{T}}\mathbf{L} \, d\Omega = \sum_{j=1}^{n_{gi}} w_{<j>}\mathbf{B}_{<j>}^{\mathrm{T}}\mathbf{L}_{<j>}, \tag{67}$$

$$\mathbf{k}_{qu} = \left[\mathbf{M}_{<j>}\mathbf{B}_{<j>}\right], \tag{68}$$

$$\mathbf{k}_{qq} = \mathrm{DIAG}\left[N_{<j>}\right], \tag{69}$$

$$\mathbf{r}_f = \mathbf{f} - \int_{\Omega_e} \mathbf{B}^{\mathrm{T}}\boldsymbol{\sigma} \, d\Omega = \mathbf{f} - \sum_{j=1}^{n_{gi}} w_{<j>}\mathbf{B}_{<j>}^{\mathrm{T}}\boldsymbol{\sigma}_{<j>}, \tag{70}$$

$$\mathbf{r}_g = \left\{-g_{<j>}\right\}. \tag{71}$$

Here, $\mathbf{k}_{uu}$, $\mathbf{k}_{uq}$, $\mathbf{k}_{qu}$, and $\mathbf{k}_{qq}$ denote the stiffness matrices, $\mathbf{r}_f$ and $\mathbf{r}_g$ are the residual vectors for the external force and the yield condition, respectively, $\mathbf{B}$ represents the displacement–strain matrix, $\mathbf{D}$, $\mathbf{L}$, and $\mathbf{M}$ are the matrices constructed from the fourth-order tensor $\mathbf{C}$ in (47), the second-order tensors L and M in (48) and (49), respectively, and $\mathbf{k}_{qq}$ is a $n_{gi} \times n_{gi}$

diagonal matrix whose diagonal component is N in (50). In addition, $\mathbf{f}$ is the external force vector corresponding to the degrees of freedom for the nodes, $\boldsymbol{\sigma}$ is the vector form of the stress tensor $\boldsymbol{\sigma}$, and $\mathbf{r}_g$ is the vector form of the residual for the yield condition calculated at the previous iteration. Noted that the subscript j in angle brackets indicates quantities evaluated at jth Gauss integration point in an element and $w_{<j>}$ is the weighting factor at jth Gauss integration point. Substituting from (66) to (71) into (64) and (65), the element stiffness matrix $\mathbf{k}$ and the element residual force vector $\mathbf{r}$ can be rewritten as

$$
\begin{aligned}
\mathbf{k} &= \mathbf{k}_{uu} - \mathbf{k}_{uq}\mathbf{k}_{qq}^{-1}\mathbf{k}_{qu} \\
&= \sum_{j=1}^{n_{gi}} w_{<j>}\mathbf{B}_{<j>}^{T}\mathbf{D}_{<j>}\mathbf{B}_{<j>} - \sum_{j=1}^{n_{gi}} w_{<j>}\mathbf{B}_{<j>}^{T}\mathbf{L}_{<j>}N_{<j>}^{-1}\mathbf{M}_{<j>}\mathbf{B}_{<j>} \\
&= \sum_{j=1}^{n_{gi}} w_{<j>}\mathbf{B}_{<j>}^{T}\left(\mathbf{D}_{<j>} - N_{<j>}^{-1}\mathbf{L}_{<j>}\mathbf{M}_{<j>}\right)\mathbf{B}_{<j>} \\
&= \int_{\Omega_e}\mathbf{B}^{T}\mathbf{D}^{ep}\mathbf{B}\,d\Omega,
\end{aligned}
\tag{72}
$$

$$
\begin{aligned}
\mathbf{r} &= \mathbf{r}_f - \mathbf{k}_{uq}\mathbf{k}_{qq}^{-1}\mathbf{r}_g \\
&= \mathbf{f} - \sum_{j=1}^{n_{gi}} w_{<j>}\mathbf{B}_{<j>}^{T}\boldsymbol{\sigma}_{<j>} - \sum_{j=1}^{n_{gi}} w_{<j>}\mathbf{B}_{<j>}^{T}\mathbf{L}_{<j>}\left(-N_{<j>}^{-1}g_{<j>}\right) \\
&= \mathbf{f} - \int_{\Omega_e}\mathbf{B}^{T}\boldsymbol{\sigma}\,d\Omega - \int_{\Omega_e}\mathbf{B}^{T}\boldsymbol{\sigma}_g\,d\Omega,
\end{aligned}
\tag{73}
$$

where $\mathbf{D}^{ep}$ is the material modulus matrix constructed from the fourth-order tensor $\mathbf{C}^{ep}$ in (54) and $\boldsymbol{\sigma}_g$ is the vector form of the stress corrector $\boldsymbol{\sigma}_g$ in (53).

Within the proposed approach, the convergence criteria should be defined, similarly to the general coupled problems. Thus, when both the criterion of the convergence for the equilibrium equation and that for the yield condition are satisfied simultaneously, the solution has sufficiently converged. As for the equilibrium equation, the global force vectors are constructed from element contributions as

$$
\mathbf{F}^{int} = \overset{n_{el}}{\underset{e=1}{\mathbf{A}}}\left(\int_{\Omega_e}\mathbf{B}^{T}\boldsymbol{\sigma}\,d\Omega\right),
\tag{74}
$$

$$
\mathbf{F}^{ext} = \overset{n_{el}}{\underset{e=1}{\mathbf{A}}}\left(\mathbf{f}\right),
\tag{75}
$$

where $\mathbf{F}^{int}$ and $\mathbf{F}^{ext}$ are the global internal and external force vectors, respectively. Hence, the global residual force vector $\mathbf{R}_f$ in (59) can be rewritten as

$$
\mathbf{R}_f = \overset{n_{el}}{\underset{e=1}{\mathbf{A}}}\left(\mathbf{r}_f\right) = \overset{n_{el}}{\underset{e=1}{\mathbf{A}}}\left(\mathbf{f} - \int_{\Omega_e}\mathbf{B}^{T}\boldsymbol{\sigma}\,d\Omega\right) = \mathbf{F}^{ext} - \mathbf{F}^{int},
\tag{76}
$$

and the criterion of the convergence for the equilibrium equation can be expressed using the global residual force vector $\mathbf{R}_f$ as

$$
||\mathbf{R}_f||_2 \leq h_f||\mathbf{F}^{ext}||_2,
\tag{77}
$$

where h_f is the tolerance of the convergence to be set as a small number and

$$
||\mathbf{R}_f||_2 = \left(\mathbf{R}_f^{T}\mathbf{R}_f\right)^{\frac{1}{2}}, \quad ||\mathbf{F}^{ext}||_2 = \left(\mathbf{F}^{ext\,T}\mathbf{F}^{ext}\right)^{\frac{1}{2}}.
\tag{78}
$$

On the other hand, the criterion of the convergence for the yield condition can be represented using the global residual vector $\mathbf{R}_g$ in (60) as

$$
||\mathbf{R}_g||_2 \leq h_g,
\tag{79}
$$

where h_g is the tolerance of the convergence to be chosen as a small number and

$$||\mathbf{R}_g||_2 = \left(\mathbf{R}_g{}^{\mathrm{T}}\mathbf{R}_g\right)^{\frac{1}{2}}. \tag{80}$$

It should be noted that, if the criterion of the convergence for the yield condition (79) is satisfied, the stress corrector σ_g in (53) should be sufficiently small. Details of the global Newton procedure are summarized for convenience in Box 2.

3.6 | Stress state in elastic domain

Here, the situation that the stress state remains elastic state during the deformation within a typical time step $[t_n, t_{n+1}]$ is considered. In this situation, the increment of the consistency parameter at ith iteration must be zero (refer Box 2), as follows:

$$\Delta\gamma^{(i)} \equiv 0. \tag{81}$$

In the proposed approach, the unit normal field to the von Mises cylinder can be calculated in (27), if the stress state lies in the elastic domain. However, in the situation which the stress state during the deformation lies in $\mathrm{int}(\mathbb{E}_\sigma)$, the unit normal field to the von Mises yield surface cannot be expressed and should be defined as

$$\boldsymbol{n}(\boldsymbol{u}_{n+1}^{(i)}, \gamma_{n+1}^{(i)}) \equiv \mathbf{0}, \tag{82}$$

since the stress state do not exist on the yield surface $\partial\mathbb{E}_\sigma$ (refer Box 1). Therefore, substituting (81) and (82) into (54), the tangent moduli $\mathbf{C}^{\mathrm{ep}}$ coincide with the elastic tensor $\mathbf{C}^{\mathrm{e}}$ (refer Boxes 1 and 2) as

$$\mathbf{C}^{\mathrm{ep}} = \mathbf{C}^{\mathrm{e}}. \tag{83}$$

On the other hand, when the yield condition g is calculated as negative, which means that the stress state lies in the elastic domain, the stress corrector σ_g must be zero as derived by substituting (82) into (53). In addition, in the elastic state ($g < 0$), the yield condition is modified (refer Box 1) as

$$g(\boldsymbol{u}_{n+1}^{(i)}, \gamma_{n+1}^{(i)}) \equiv 0. \tag{84}$$

Therefore, the yield condition in the elastic state, which is calculated at each integration point, does not affect the criterion of the convergence for the yield condition (79).

Box 2 Procedure of updating variables in finite element analysis

1. Initialize.

$$\begin{aligned}
\Delta\gamma^{(0)} &= 0 \\
g(\boldsymbol{u}_{n+1}^{(0)}, \gamma_{n+1}^{(0)}) &= 0 \\
\varepsilon^{\mathrm{p}}(\boldsymbol{u}_{n+1}^{(0)}, \gamma_{n+1}^{(0)}) &= \varepsilon^{\mathrm{p}}(\boldsymbol{u}_n, \gamma_n) \\
\alpha(\gamma_{n+1}^{(0)}) &= \alpha(\gamma_n) \\
\beta(\boldsymbol{u}_{n+1}^{(0)}, \gamma_{n+1}^{(0)}) &= \beta(\boldsymbol{u}_n, \gamma_n) \\
\boldsymbol{n}(\boldsymbol{u}_{n+1}^{(0)}, \gamma_{n+1}^{(0)}) &= \boldsymbol{n}(\boldsymbol{u}_n, \gamma_n)
\end{aligned}$$

2. Compute tangent moduli for first calculation from equilibrium state.

$$\mathbf{C}^{\mathrm{ep}}(\boldsymbol{u}_{n+1}^{(0)}, \gamma_{n+1}^{(0)}) = \mathbf{C}(\boldsymbol{u}_{n+1}^{(0)}, \gamma_{n+1}^{(0)}) - N^{-1}(\gamma_{n+1}^{(0)})\boldsymbol{L}(\boldsymbol{u}_{n+1}^{(0)}, \gamma_{n+1}^{(0)}) \otimes \boldsymbol{M}(\boldsymbol{u}_{n+1}^{(0)}, \gamma_{n+1}^{(0)})$$

where

$$\mathbf{C}(\boldsymbol{u}_{n+1}^{(0)}, \gamma_{n+1}^{(0)}) = \mathbf{C}^{\mathrm{e}} - \mathbf{C}^{\mathrm{e}} : \left\{ \frac{2\mu\Delta\gamma^{(0)}}{|\xi^{\mathrm{tr}}|} \left[\mathbf{I} - \frac{1}{3}\mathbf{1}\otimes\mathbf{1} - \boldsymbol{n}(\boldsymbol{u}_{n+1}^{(0)},\gamma_{n+1}^{(0)})\otimes\boldsymbol{n}(\boldsymbol{u}_{n+1}^{(0)},\gamma_{n+1}^{(0)}) \right] \right\} = \mathbf{C}^{\mathrm{e}}$$

$$\boldsymbol{L}(\boldsymbol{u}_{n+1}^{(0)},\gamma_{n+1}^{(0)}) = -2\mu\boldsymbol{n}(\boldsymbol{u}_{n+1}^{(0)},\gamma_{n+1}^{(0)}) = -2\mu\boldsymbol{n}(\boldsymbol{u}_n,\gamma_n)$$

$$\boldsymbol{M}(\boldsymbol{u}_{n+1}^{(0)},\gamma_{n+1}^{(0)}) = 2\mu\boldsymbol{n}(\boldsymbol{u}_{n+1}^{(0)},\gamma_{n+1}^{(0)}) = 2\mu\boldsymbol{n}(\boldsymbol{u}_n,\gamma_n)$$

$$N(\gamma_{n+1}^{(0)}) = -\left\{ 2\mu + \frac{2}{3}\left[H' + K'(\gamma_{n+1}^{(0)}) \right] \right\} = -\left\{ 2\mu + \frac{2}{3}\left[H' + K'(\gamma_n) \right] \right\}$$

3. Iterate.

DO UNTIL: $\left\{ ||\mathbf{R}_{\mathrm{f}}||_2 \le h_{\mathrm{f}}||\mathbf{F}^{\mathrm{ext}}||_2 \ \& \ ||\mathbf{R}_{\mathrm{g}}||_2 \le h_{\mathrm{g}} \right\}$ OR $\{||\mathbf{U}||_2 \le \mathrm{TOL} \ \& \ ||\mathbf{Q}||_2 \le \mathrm{TOL}\}$,

(TOL is the word employed to set approximate zero.)

$k \leftarrow k+1$

3.1. Compute $\delta\boldsymbol{u}^{(k+1)}$ to solve equilibrium equation for overall structure.

$$\mathbf{KU} = \mathbf{R}$$

3.2. Compute $\delta\gamma^{(k+1)}$ from $\delta\boldsymbol{u}^{(k+1)}$ at either material point or element level.

At material point:

$$\delta\gamma^{(k+1)} = -N^{-1}(\gamma_{n+1}^{(k)})\boldsymbol{M}(\boldsymbol{u}_{n+1}^{(k)},\gamma_{n+1}^{(k)}) : \boldsymbol{\varepsilon}(\delta\boldsymbol{u}^{(k+1)}) - N^{-1}(\gamma_{n+1}^{(k)}) \cdot g(\boldsymbol{u}_{n+1}^{(k)},\gamma_{n+1}^{(k)})$$

At element level (internal variables $\mathbf{q}$; displacements $\mathbf{u}$):

$$\mathbf{q} = \mathbf{k}_{\mathrm{qq}}^{-1}\left(\mathbf{r}_{\mathrm{g}} - \mathbf{k}_{\mathrm{qu}}\mathbf{u} \right)$$

3.3. Update variables.

$$\Delta\boldsymbol{u}^{(k+1)} = \Delta\boldsymbol{u}^{(k)} + \delta\boldsymbol{u}^{(k+1)}$$
$$\Delta\gamma^{(k+1)} = \Delta\gamma^{(k)} + \delta\gamma^{(k+1)}$$

IF $\Delta\gamma^{(k+1)} < 0$ THEN:

$$\Delta\gamma^{(k+1)} \equiv 0$$

ENDIF

3.4. Update state variables and stress from Box 1.

3.5. Compute internal force $\mathbf{F}^{\mathrm{int}}$.

4 | NUMERICAL EXAMPLES

Two models of cantilever beam and perforated strip in the plane strain state are chosen to illustrate the performance of the proposed approach. Its performance for the practical importance is demonstrated by comparing the rate of convergence of the proposed approach with that of the conventional return mapping algorithm. The numerical results using the proposed approach based on the block Newton method are labeled as BN, and similarly, the results calculated with the return mapping algorithm are abbreviated as RM.

In this section, the isotropic and kinematic hardening rules of the exponential type, as in Voce,[48] are employed and defined according to the expressions

$$K(\alpha) = \theta\left\{ \overline{H}\alpha + \left(\overline{K}_\infty - \overline{K}_0 \right)\left[1 - \exp\left(-\overline{\zeta}\alpha \right) \right] \right\},$$
$$H(\alpha) = (1-\theta)\left\{ \overline{H}\alpha + \left(\overline{K}_\infty - \overline{K}_0 \right)\left[1 - \exp\left(-\overline{\zeta}\alpha \right) \right] \right\},$$

where $\theta \in [0, 1]$ is a material parameter driving the ratio between the isotropic/kinematic hardening laws, $\overline{H} \geq 0$, $\overline{K}_\infty \geq \overline{K}_0 > 0$, and $\overline{\zeta} \geq 0$ are material constants.
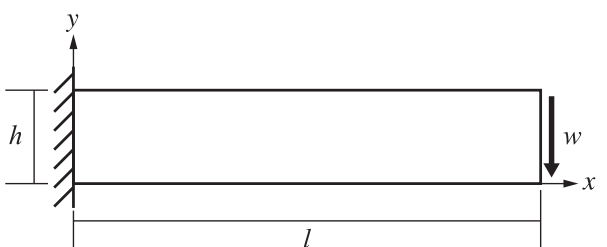
All the numerical examples described below employ a four-node quadrilateral element with bilinear isoparametric interpolations for the displacement field. Here, the incremental time Δt can be represented as $\Delta t = 1/n_{ls}$, where n_{ls} denotes the number of the total loading step in the incremental analysis.

In the proposed approach, the convergence is checked by the criteria of both (77) and (79) simultaneously. On the other hand, in the conventional return mapping algorithm, the convergence is judged when the criterion in (77) is satisfied, and it should be noted that the local iterative calculation[45,46] which corrects the stress state at each integration point. In this section, we set the values of tolerance as $h_f = 10^{-6}$ and $h_g = 10^{-6}$, respectively. Note that, in the conventional return mapping algorithm,[45,46] the criterion of the yield condition at each integration point is $\|g\|_1 \leq \|\mathbf{R}_g\|_{cr}$ in the local iterative calculation for determining the consistency parameter, where $\|\bullet\|_1$ denotes the L_1 norm and the criterion is $\|\mathbf{R}_g\|_{cr} = 10^{-6}$. Here, the criterion for the yield condition (79) in the proposed approach can be regarded as a more severe condition than that for the conventional return mapping algorithm, since the residual for the yield condition is expressed by the L_2 norm calculated at each integration point as shown in (80). In this work, the rate of convergence is verified considering the difference of the above criteria. In addition, no tolerance on the L_2 norm of $\mathbf{U}$ and $\mathbf{Q}$ in Box 2 is employed in this section.

4.1 | Cantilever beam subjected to bending with applied displacement

A cantilever beam is clamped on one end and applied displacement on the other end. The geometry, material data, and boundary conditions are given in Figure 1. Here, the time interval for numerical simulation is defined by $t = [0, 1]$, and the applied displacement is increased linearly in time. This model is discretized with 50×10 elements.

Figures 2 and 3 show the distributions of the equivalent plastic strain in the final deformed configuration for $\Delta t = 0.01$ and $\Delta t = 0.00125$, respectively. As depicted in Figures 2 and 3, since the backward difference scheme is applied to both BN and RM, the numerical results of both are almost identical and the discrepancy between both results comes from the discretization error of stress integration. Thus, the proposed approach gives the numerical solutions that do not depend on the convergence paths, similarly to the conventional return mapping algorithm. In addition, Figure 4 expresses the cumulative number of iterations for convergence at each time step. It should be noted that the total number of iterations is written in each graph legend. As shown in Figure 4, the cumulative number of iterations for BN is larger than that of RM. However, with respect to the increasing tendency of the cumulative number, minor difference is confirmed between both BN and RM. It should be noted that the conventional return mapping

FIGURE 1 Geometry and material data of a cantilever beam

Geometry:
$h = 1$ mm
$l = 5$ mm

Applied displacement:
$w = 1$ mm

Material:
$E = 2.1 \times 10^5$ N/mm^2
$v = 0.3$
$\sigma_Y = 6.0 \times 10^2$ N/m^2
$\theta = 0$
$\bar{H} = 2.1 \times 10^3$ N/mm^2
$\bar{\zeta} = 0$
$\bar{K}_0 = 6.0 \times 10^2$ N/mm^2
$\bar{K}_\infty = 6.0 \times 10^2$ N/mm^2
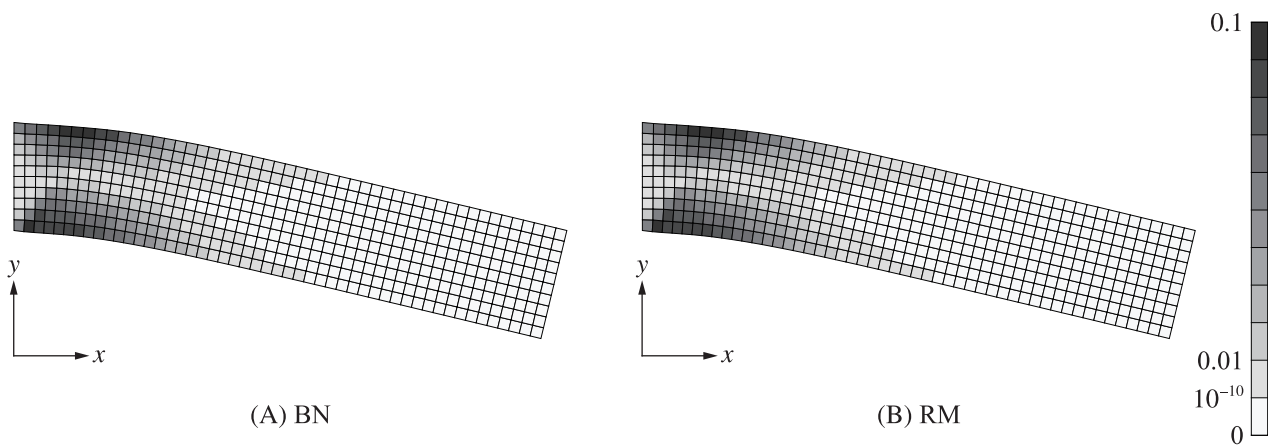
FIGURE 2 Equivalent plastic strain distributions in the final deformation diagram of a cantilever beam for $\Delta t = 0.01$; (A) BN and (B) RM
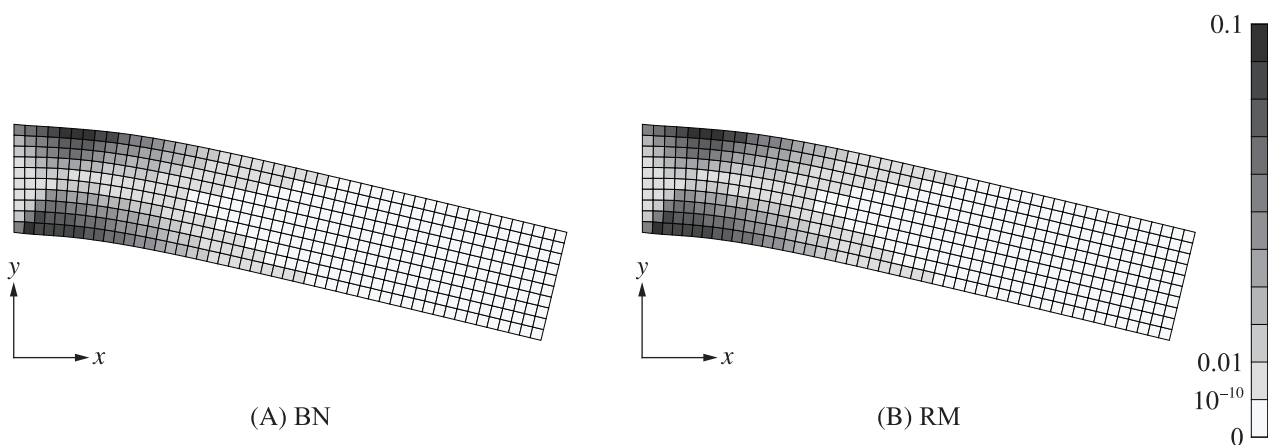

FIGURE 3 Equivalent plastic strain distributions in the final deformation diagram of a cantilever beam for $\Delta t = 0.00125$; (A) BN and (B) RM
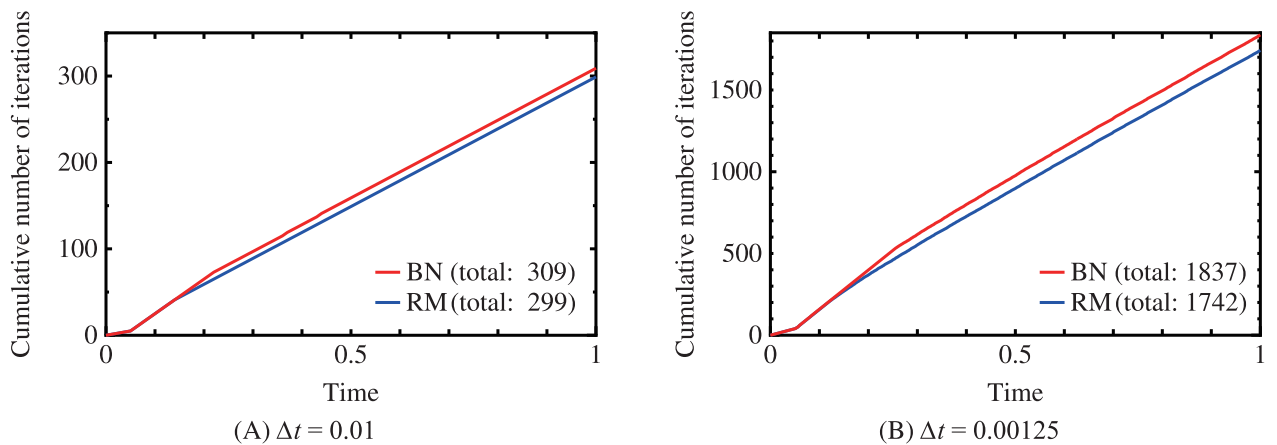

FIGURE 4 Cumulative number of iterations for each time step of a cantilever beam; (A) $\Delta t = 0.01$ and (B) $\Delta t = 0.00125$
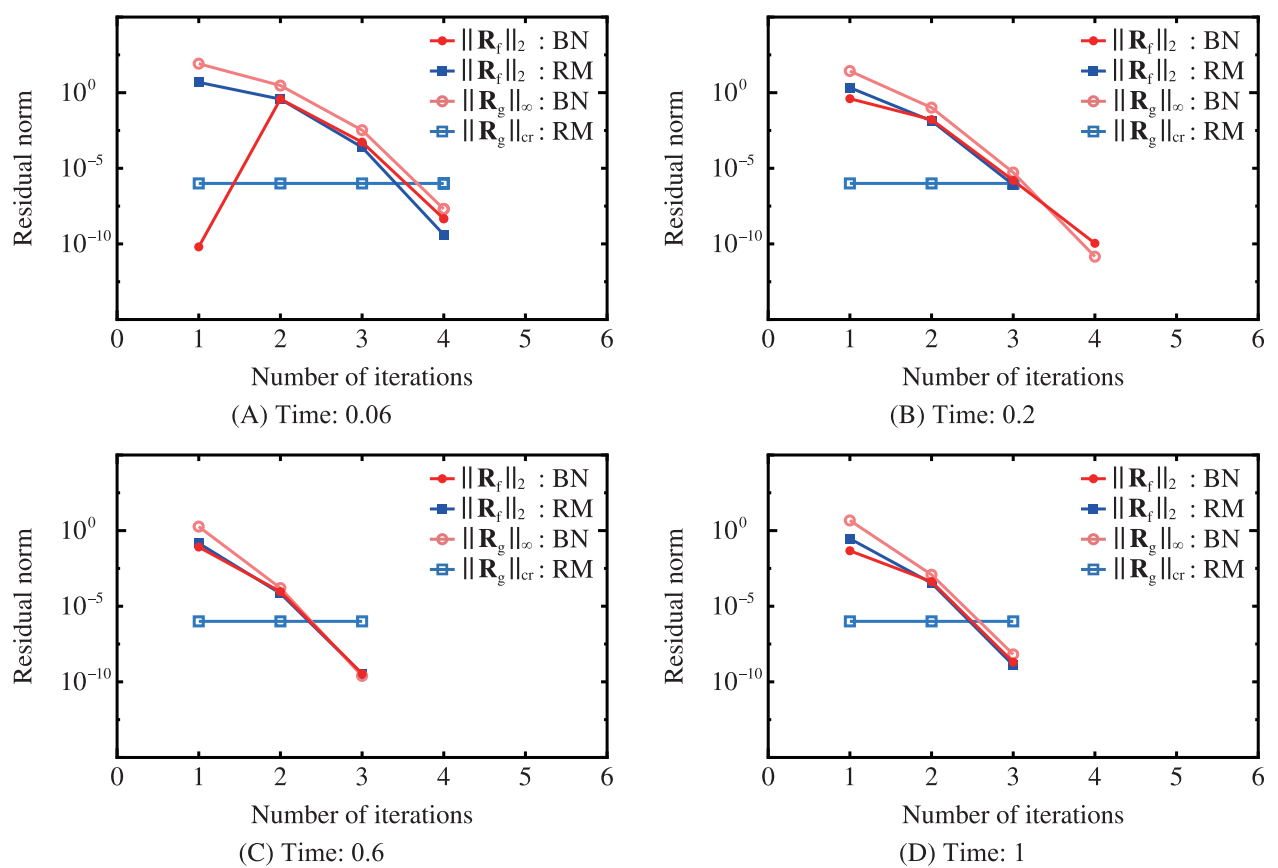
FIGURE 5 Residual norm of a cantilever beam for $\Delta t = 0.01$; (A) $t = 0.06$, (B) $t = 0.2$, (C) $t = 0.6$, and (D) $t = 1$

algorithm requires local iterative calculation at each integration point that is not represented in the cumulative number given in Figure 4. On the other hand, the proposed approach does not include local iterative calculation at each integration point.

The changes in the residual norm until convergence for both the proposed approach and the conventional return mapping algorithm are shown in Figures 5 and 6. Here, $||\bullet||_2$ and $||\bullet||_\infty$ denote the L_2 norm, which is calculated in (78), and the L_∞ norm, respectively. It should be noted that the convergence for the yield condition in the proposed approach is evaluated using the L_2 norm represented in (80). For this convergence criteria, the residuals to convergence behave as shown in these figures. In addition, for the conventional return mapping algorithm, the convergence criterion of the yield condition for the local iterative calculation at each integration point is also depicted in Figures 5 and 6. Figures 5(A) and 6(A) describe the numerical results for the first time step that required multiple iterations to converge. Hence, in focus on the numerical results for BN in those figures, the residual norm $||\mathbf{R}_f||_2$ is determined to be sufficiently small in the first calculation; however, the residual norm $||\mathbf{R}_g||_\infty$ has a size that cannot be ignored. At the second iteration, since the stress corrector σ_g, which includes the residual norm for the yield condition, is added to the residual force vector $\mathbf{R}$ for solving the equilibrium equation, the residual norm $||\mathbf{R}_f||_2$ may become large. As seen from Figures 5 and 6, the rate of convergence of the proposed approach can be regarded as the same as that of the conventional return mapping algorithm. At each time step, the number of iterations in the proposed approach is at most one more than that in the conventional return mapping algorithm. Therefore, no significant difference can be observed in the increasing tendency of the cumulative number of iterations in Figure 4.

4.2 | Perforated strip

We consider the plane strain problem of an infinitely long rectangular strip.[45,46] The geometry and boundary conditions are described in Figure 7. On account of symmetry, one-fourth of the strip is modeled and discretized as shown in Figure 7.

(A) Time: 0.0525

(B) Time: 0.2

(C) Time: 0.6

(D) Time: 1
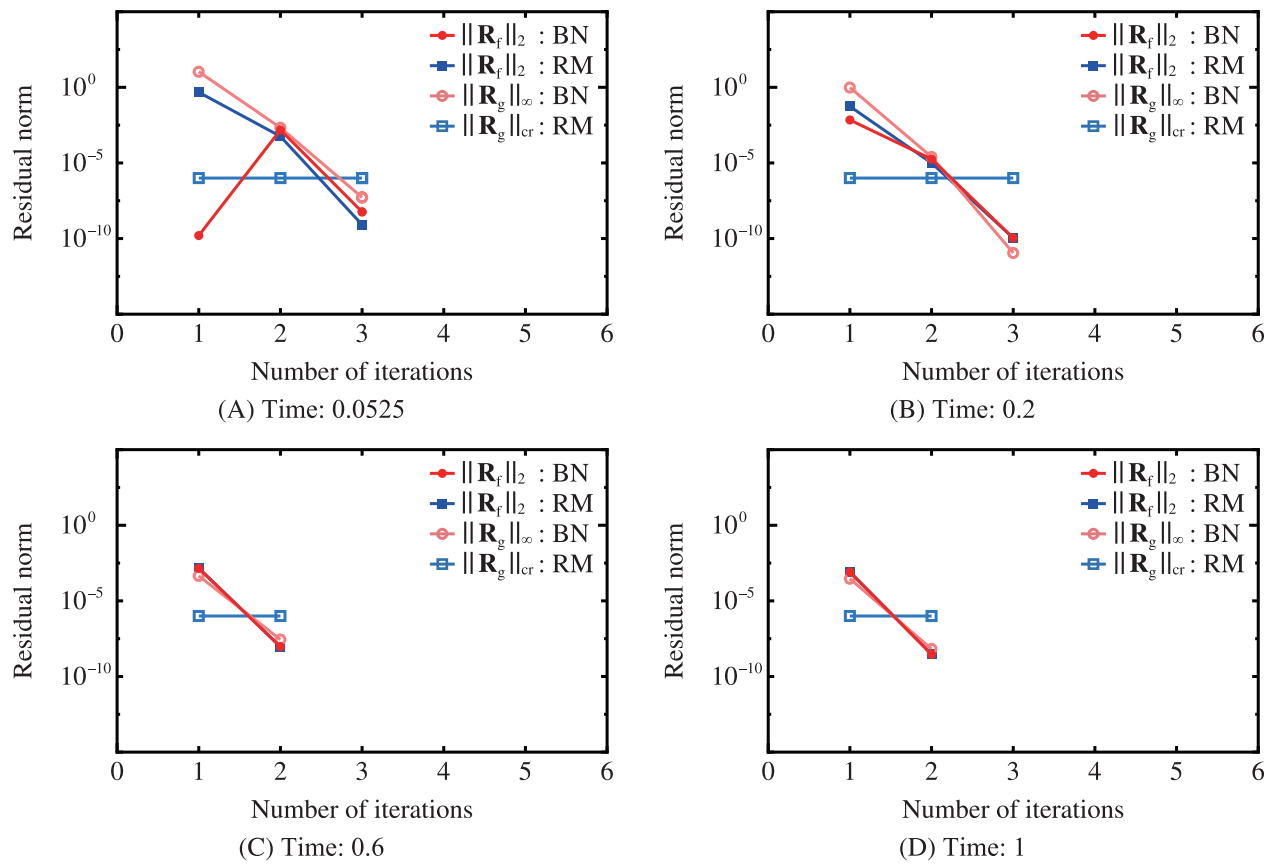
FIGURE 6 Residual norm of a cantilever beam for $\Delta t = 0.00125$; (A) $t = 0.0525$, (B) $t = 0.2$, (C) $t = 0.6$, and (D) $t = 1$
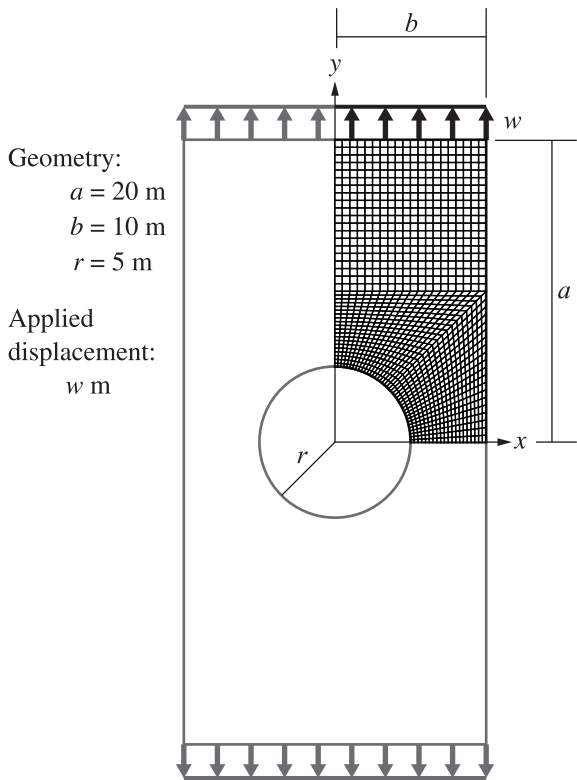
FIGURE 7 Geometry and material data of a plane strain strip with a circular hole

Geometry:
$a = 20$ m
$b = 10$ m
$r = 5$ m

Applied displacement:
w m

4.2.1 | Uniaxial extension with perfect plasticity

The material data are set as follows:

$$
\begin{aligned}
E &= 7.0 \times 10^7 \text{ N/m}^2, & \nu &= 0.2, \\
\sigma_Y &= 2.43 \times 10^5 \text{ N/m}^2, & \theta &= 1, \\
\overline{H} &= 0 \text{ N/m}^2, & \overline{\zeta} &= 0, \\
\overline{K}_0 &= 2.43 \times 10^5 \text{ N/m}^2, & \overline{K}_\infty &= 2.43 \times 10^5 \text{ N/m}^2.
\end{aligned}
$$

Here, the time interval for numerical simulation is defined by $t = [0, 1]$, and the applied displacement w is increased linearly in time up to the value of 0.5.

Figures 8 and 9 represent the distributions of the equivalent plastic strain in the final deformed configuration for $\Delta t = 0.01$ and $\Delta t = 0.00125$, respectively. As depicted in Figures 8 and 9, the numerical results of both are almost identical, since the backward difference scheme is applied to both BN and RM. Similarly to Section 4.1, the discrepancy between both results comes from the discretization error of stress integration. Thus, the proposed approach does not exhibit dependency of the numerical solutions on convergence paths, similarly to the conventional return mapping algorithm. In
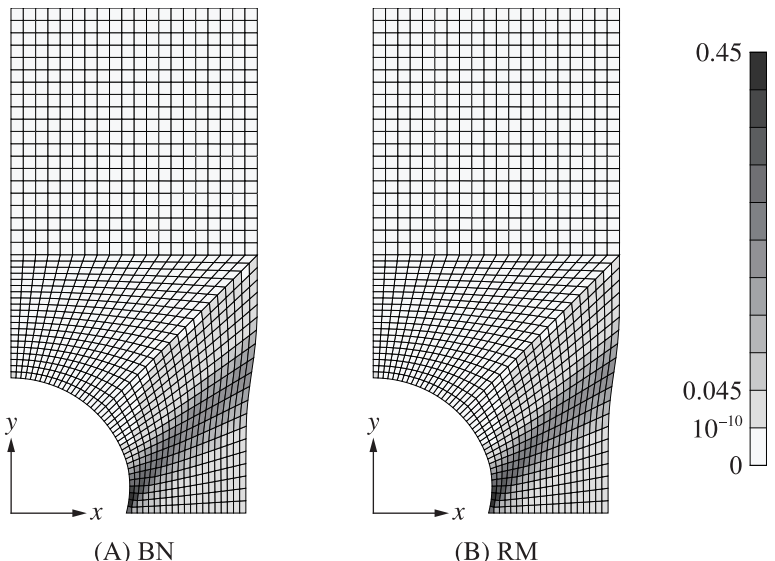

FIGURE 8 Equivalent plastic strain distributions in the final deformation diagram of a plane strain strip of perfect plasticity with a circular hole under uniaxial extension for $\Delta t = 0.01$; (A) BN and (B) RM

(A) BN   (B) RM

FIGURE 9 Equivalent plastic strain distributions in the final deformation diagram of a plane strain strip of perfect plasticity with a circular hole under uniaxial extension for $\Delta t = 0.00125$; (A) BN and (B) RM

(A) BN   (B) RM

addition, Figure 10 describes the cumulative number of iterations for convergence at each time step. Note that the total number of iterations is written in each graph legend. As shown in Figure 10, the cumulative number of iterations for BN is larger than that of RM, similarly to Section 4.1. Note that the conventional return mapping algorithm includes local iterative calculation at each integration point. On the other hand, the proposed approach does not require local iterative calculation.

The changes in the residual norm until convergence for both the proposed approach and the conventional return mapping algorithm are given in Figures 11 and 12. For this convergence criteria, the residuals to convergence have the
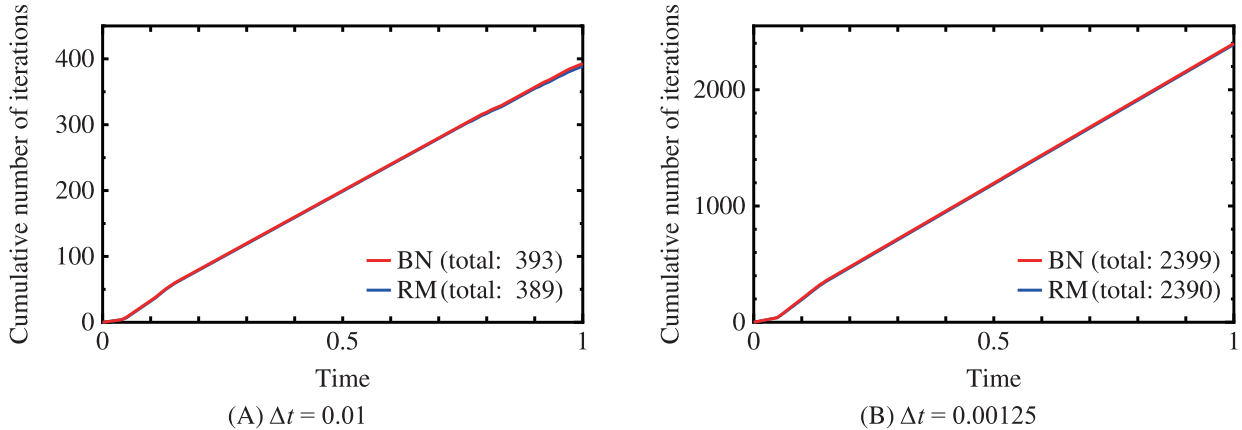
FIGURE 10 Cumulative number of iterations for each time step of a plane strain strip of perfect plasticity with a circular hole under uniaxial extension; (A) $\Delta t = 0.01$ and (B) $\Delta t = 0.00125$
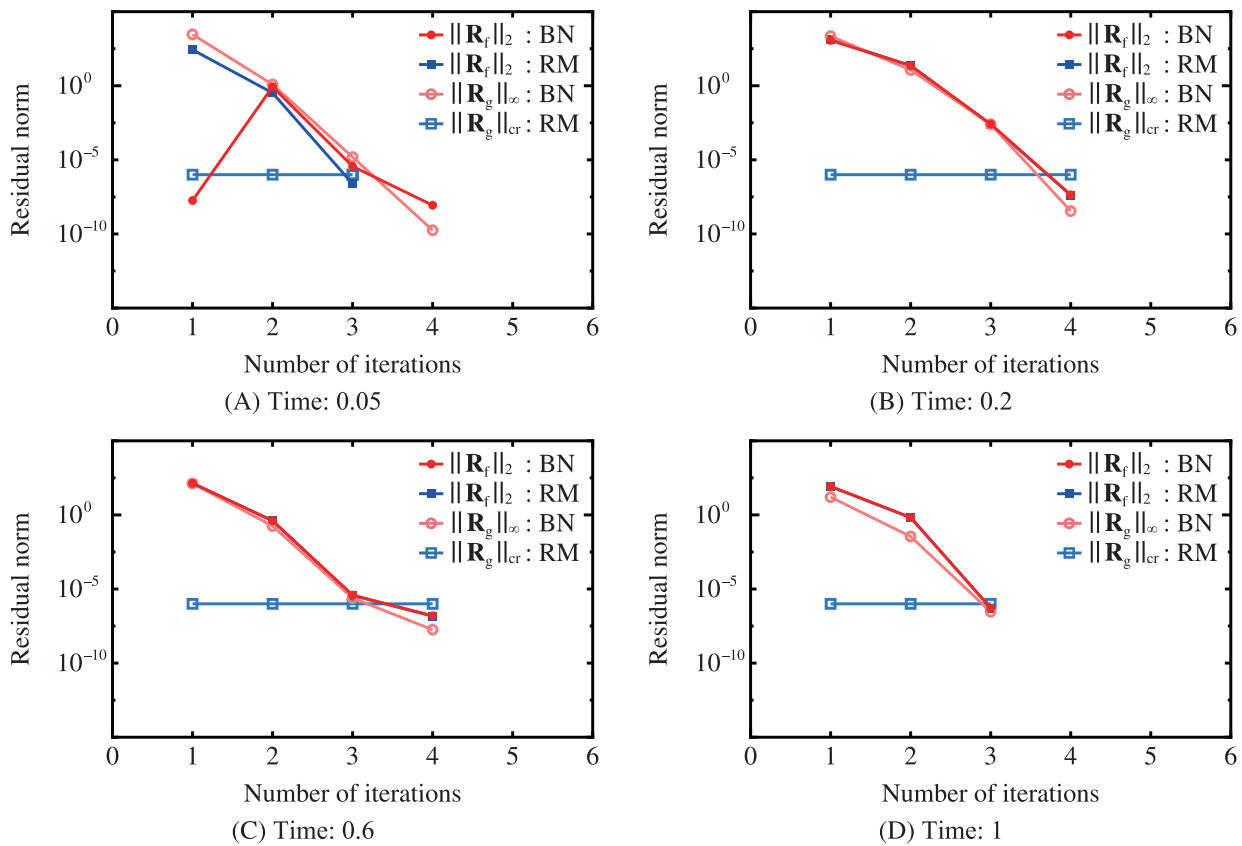
FIGURE 11 Residual norm of a plane strain strip of perfect plasticity with a circular hole under uniaxial extension for $\Delta t = 0.01$; (A) $t = 0.05$, (B) $t = 0.2$, (C) $t = 0.6$, and (D) $t = 1$
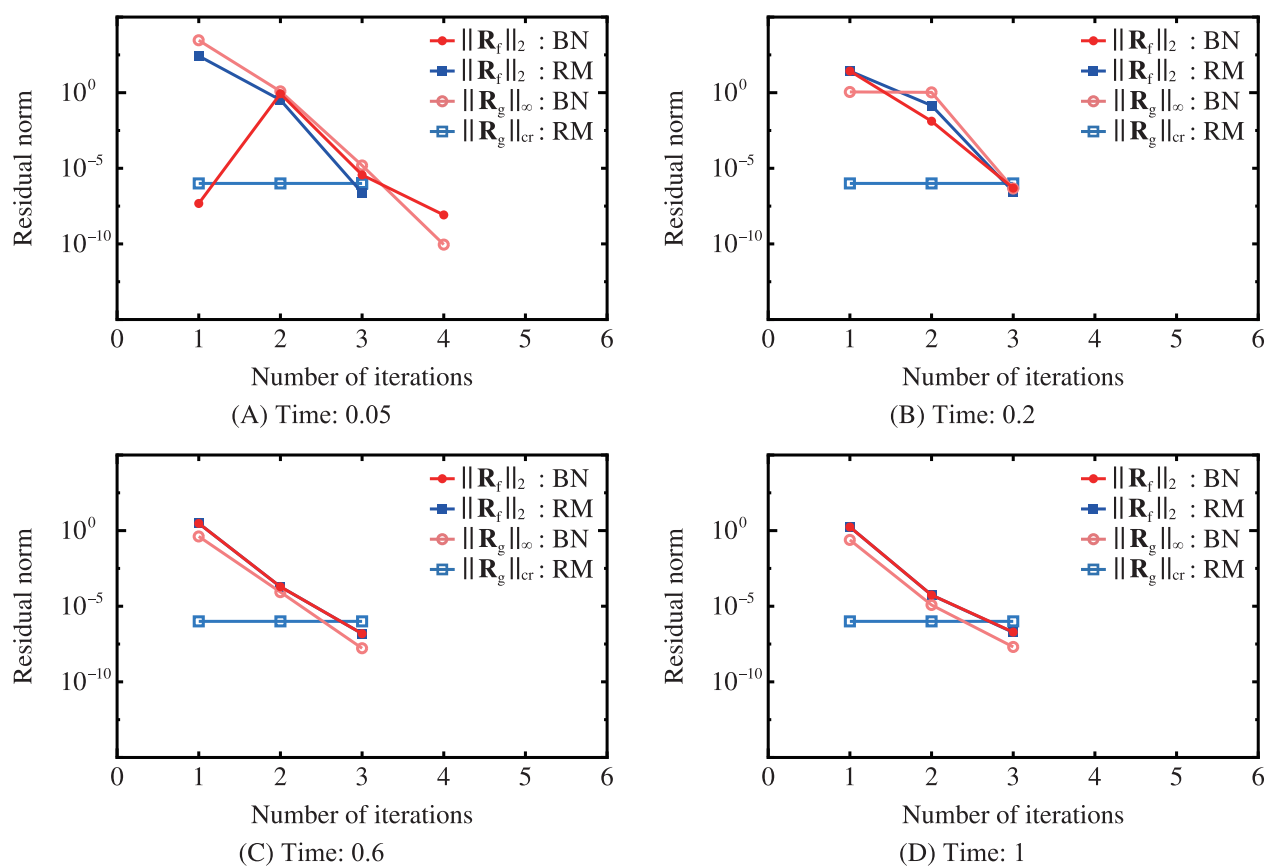
FIGURE 12 Residual norm of a plane strain strip of perfect plasticity with a circular hole under uniaxial extension for $\Delta t = 0.00125$; (A) $t = 0.05$, (B) $t = 0.2$, (C) $t = 0.6$, and (D) $t = 1$

behavior as depicted in these figures. For the conventional return mapping algorithm, the convergence criterion of the yield condition for local iterative calculation at each integration point is also shown in Figures 11 and 12. Figures 11(A) and 12(A) illustrate the numerical results for the first time step that required multiple iterations to converge. Hence, in focus on the numerical results for BN in those figures, the residual norm $\|\mathbf{R}_f\|_2$ is sufficiently small in the first calculation; however, the residual norm $\|\mathbf{R}_g\|_\infty$ has a size that cannot be ignored. At the second iteration, since the stress corrector $\boldsymbol{\sigma}_g$ must be added to the residual force vector $\mathbf{R}$ for solving the equilibrium equation, the residual norm $\|\mathbf{R}_f\|_2$ may become large. As shown in Figures 11 and 12, the rate of convergence of the proposed approach can be regarded as the same as that of the conventional return mapping algorithm. From these results, the number of iterations at each time step in the proposed approach is at most one more than that in the conventional return mapping algorithm.

4.2.2 | Uniaxial extension with hardening plasticity

The material data are given as follows:

$$
\begin{aligned}
E &= 7.0 \times 10^7 \text{ N/m}^2, & \nu &= 0.2, \\
\sigma_Y &= 2.43 \times 10^5 \text{ N/m}^2, & \theta &= 0.1, \\
\overline{H} &= 7.0 \times 10^5 \text{ N/m}^2, & \overline{\zeta} &= 0.1, \\
\overline{K}_0 &= 2.43 \times 10^5 \text{ N/m}^2, & \overline{K}_\infty &= 3.43 \times 10^5 \text{ N/m}^2.
\end{aligned}
$$

Here, the time interval for numerical simulation is defined by $t = [0, 1]$ and the applied displacement is set as same as in Section 4.2.1.

Figures 13 and 14 show the distributions of the equivalent plastic strain in the final deformed configuration for $\Delta t = 0.01$ and $\Delta t = 0.00125$, respectively. Since the backward difference scheme is applied to both BN and RM, the numerical results of both are almost identical, as represented in Figures 13 and 14. In addition, Figure 15 expresses the cumulative number of iterations for convergence at each time step. It should be noted that the total number of iterations is written in each graph legend. As depicted in Figure 15, the cumulative number of iterations for BN is considerably larger than that of RM. However, note that the amount of increase in each time step for both RM and BN is almost constant; hence, the incremental calculations for both can be regarded as stable.

The changes in the residual norm until convergence for both the proposed approach and the conventional return mapping algorithm are shown in Figures 16 and 17. For this convergence criteria, the residuals to convergence behave as described in these figures. For the conventional return mapping algorithm, the convergence criterion of the yield condition for local iterative calculation at each integration point is also given in Figures 16 and 17. Figures 16(A) and 17(A) describe the numerical results for the first time step that required multiple iterations to converge. Similarly to Section 4.2.1, in focus on the numerical results for BN in those figures, the residual norm $\|\mathbf{R}_f\|_2$ is sufficiently small in the first calculation; however, the residual norm $\|\mathbf{R}_g\|_\infty$ has a size that cannot be ignored. At the second iteration, the residual norm $\|\mathbf{R}_f\|_2$ may become large, since the stress corrector $\boldsymbol{\sigma}_g$ is added to the residual force vector $\mathbf{R}$ for solving the equilibrium equation. From Figures 16(B, C) and 17(B), it can be confirmed that the difference in convergence criteria
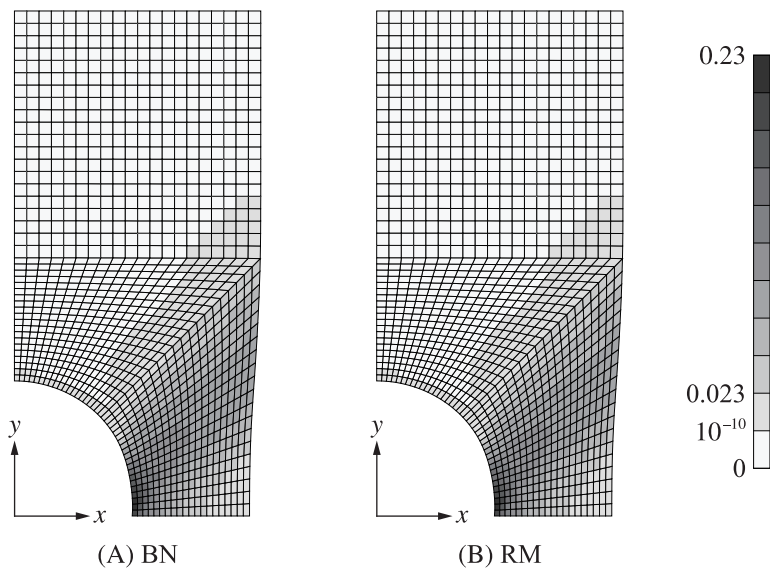
FIGURE 13 Equivalent plastic strain distributions in the final deformation diagram of a plane strain strip of hardening plasticity with a circular hole under uniaxial extension for $\Delta t = 0.01$; (A) BN and (B) RM
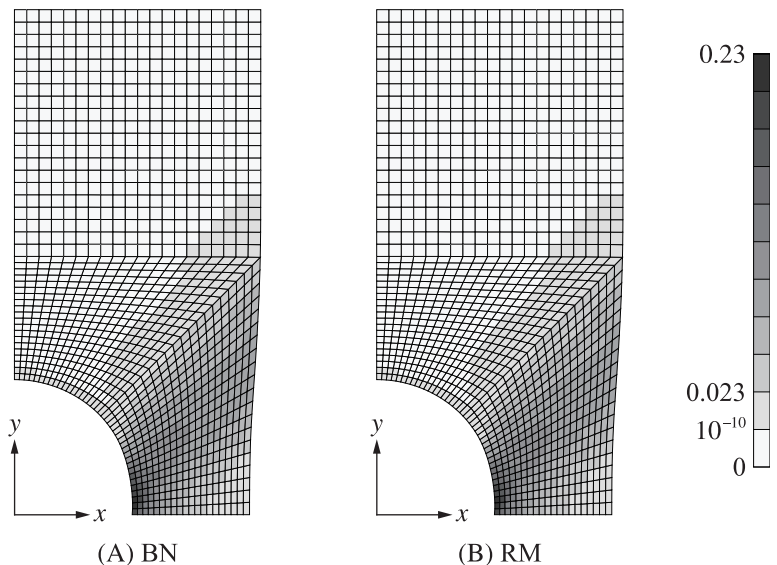

FIGURE 14 Equivalent plastic strain distributions in the final deformation diagram of a plane strain strip of hardening plasticity with a circular hole under uniaxial extension for $\Delta t = 0.00125$; (A) BN and (B) RM
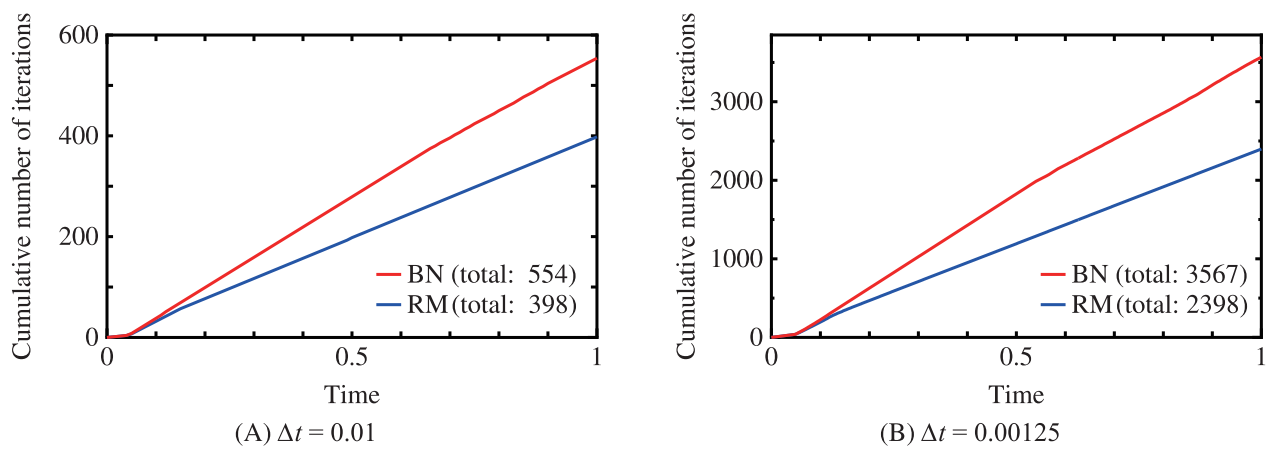
FIGURE 15 Cumulative number of iterations for each time step of a plane strain strip of hardening plasticity with a circular hole under uniaxial extension; (A) $\Delta t = 0.01$ and (B) $\Delta t = 0.00125$
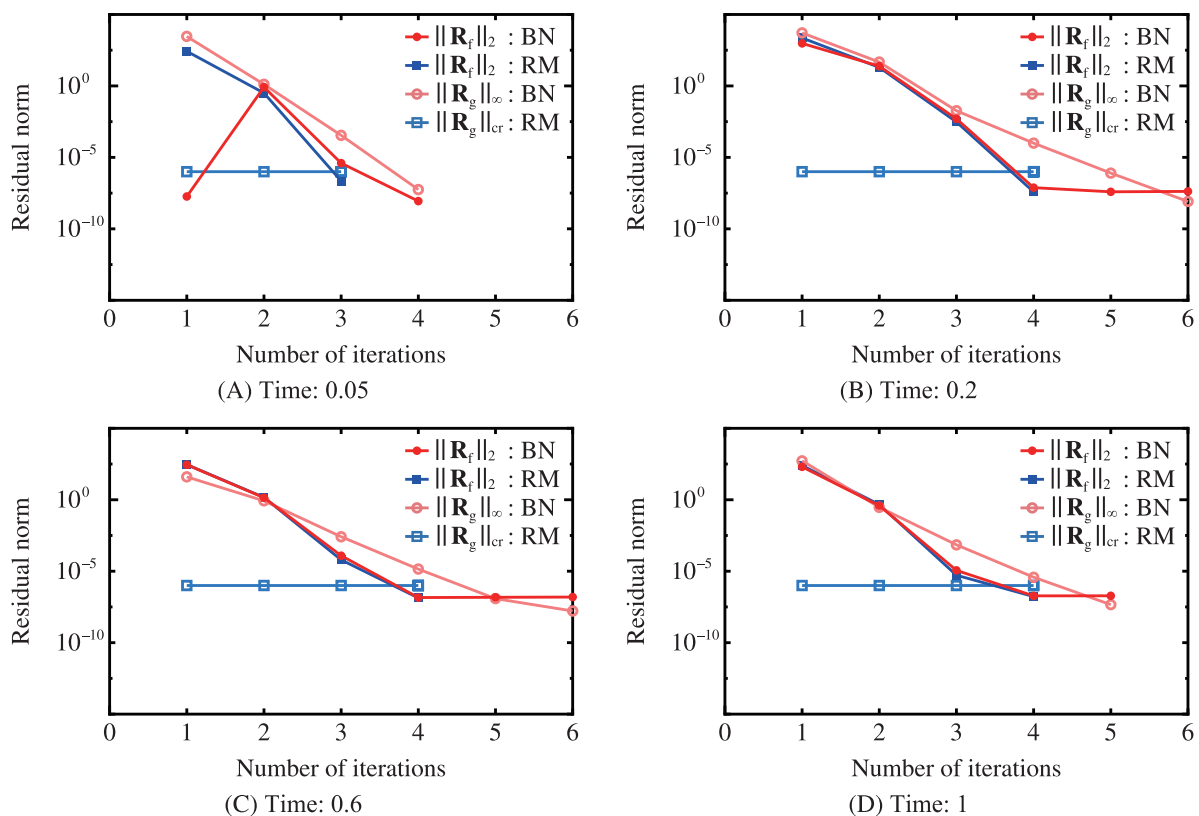

FIGURE 16 Residual norm of a plane strain strip of hardening plasticity with a circular hole under uniaxial extension for $\Delta t = 0.01$; (A) $t = 0.05$, (B) $t = 0.2$, (C) $t = 0.6$, and (D) $t = 1$

applied to BN and RM, respectively, affects the number of iterations. On the basis of the convergence criteria for RM, in the iterative calculation by BN, it can be judged that the residual norm is sufficiently small in the iteration just before converged. Hence, a large difference occurs in the cumulative number of iterations in Figure 15 due to the difference in convergence criteria. On the other hand, the rate of convergence of the proposed approach can be regarded as the same as that of the conventional return mapping algorithm, as depicted in Figures 16 and 17. In addition, the number of iterations at each time step in the proposed approach is at most two more than that in the conventional return mapping algorithm.
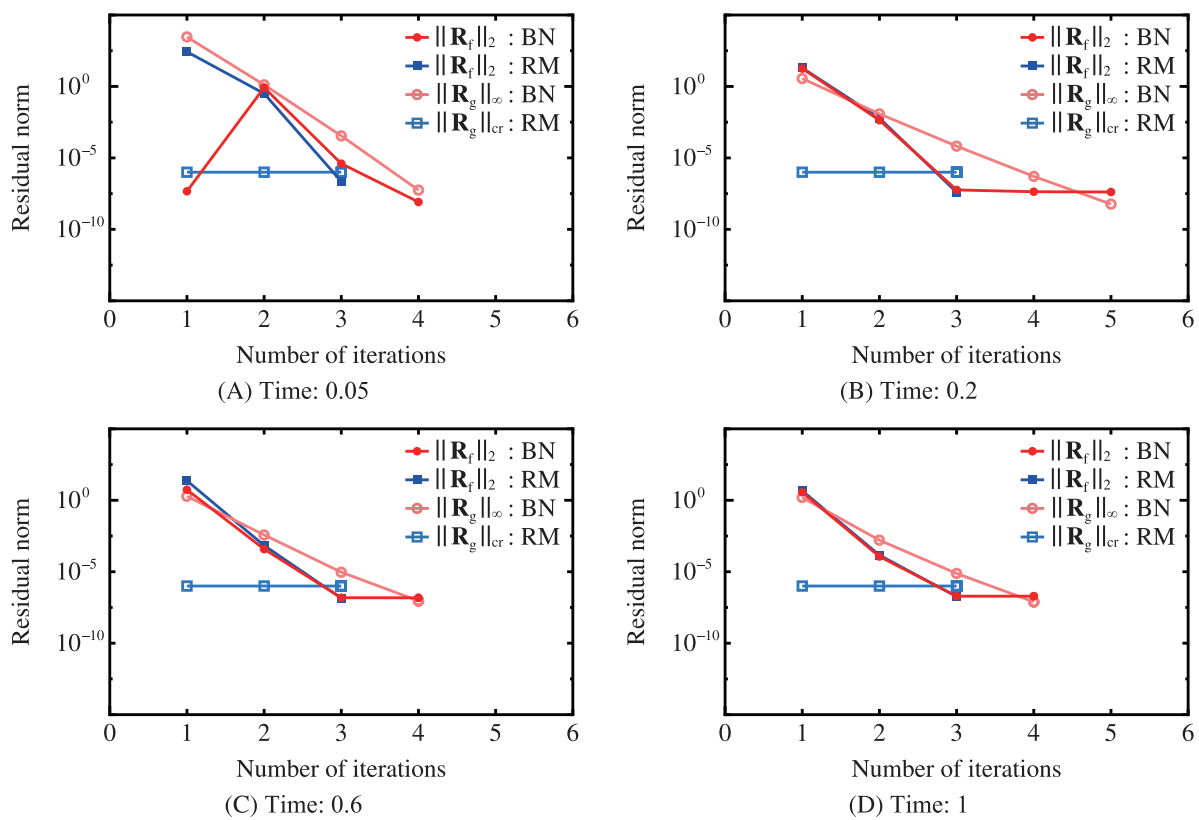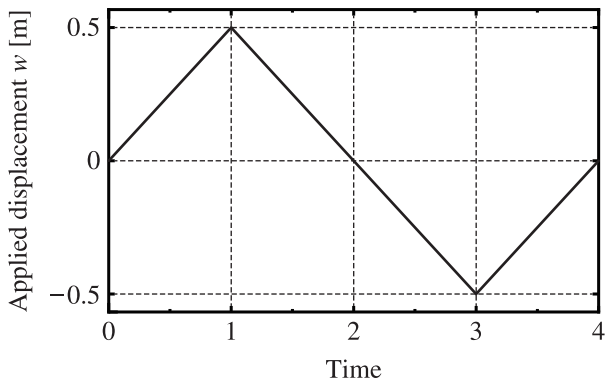
FIGURE 17 Residual norm of a plane strain strip of hardening plasticity with a circular hole under uniaxial extension for $\Delta t = 0.00125$; (A) $t = 0.05$, (B) $t = 0.2$, (C) $t = 0.6$, and (D) $t = 1$

FIGURE 18 Cyclic loading applied to a plane strain strip of hardening plasticity with a circular hole

4.2.3 | Cyclic loading with hardening plasticity

The material data are same as described in Section 4.2.2. Here, the time interval for numerical simulation is defined by $t = [0, 4]$, and the applied displacement is increased linearly in time and set as illustrated in Figure 18.

Figures 19 and 20 represent the distributions of the equivalent plastic strain in the final deformed configuration for $\Delta t = 0.01$ and $\Delta t = 0.00125$, respectively, and the numerical results of both are almost identical, since the backward difference scheme is applied to both BN and RM. In addition, Figure 21 shows the cumulative number of iterations for convergence at each time step. Note that the total number of iterations is described in each graph legend. As shown in Figure 21, the cumulative number of iterations for BN is considerably larger than that of RM, similarly to Section 4.2.2. A discussion of the difference in the cumulative number of iterations is detailed in Section 4.2.2. It should be noted that the number of iterations at each time step in the proposed approach is at most two more than that in the conventional return mapping algorithm.

FIGURE 19 Equivalent plastic strain distributions in the final deformation diagram of a plane strain strip of hardening plasticity with a circular hole under cyclic loading for $\Delta t = 0.01$; (A) BN and (B) RM


(A) BN   (B) RM
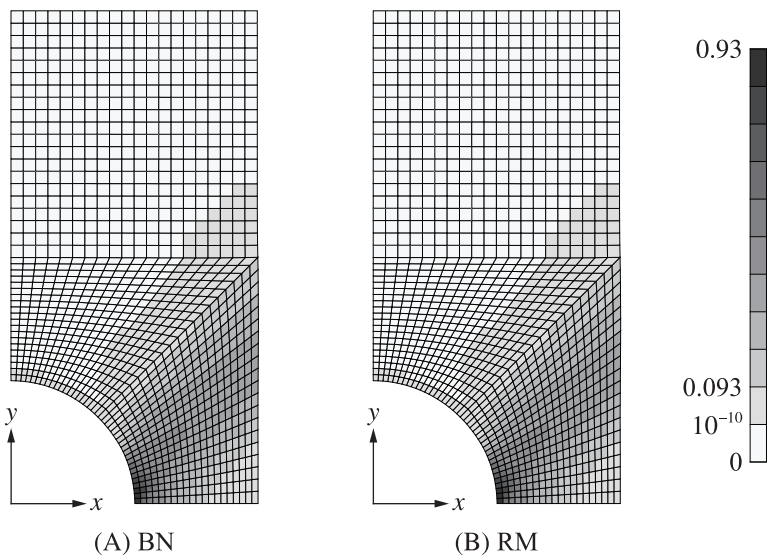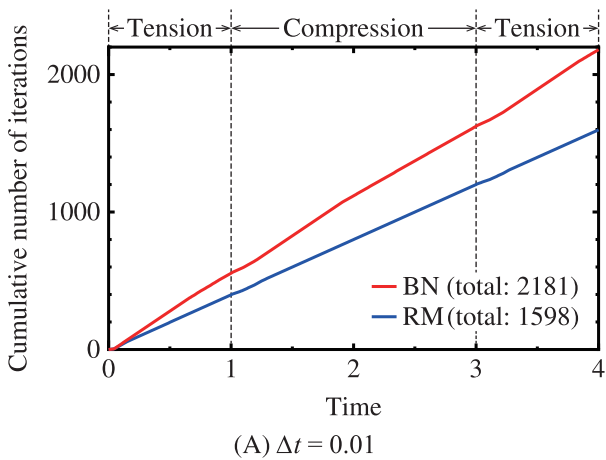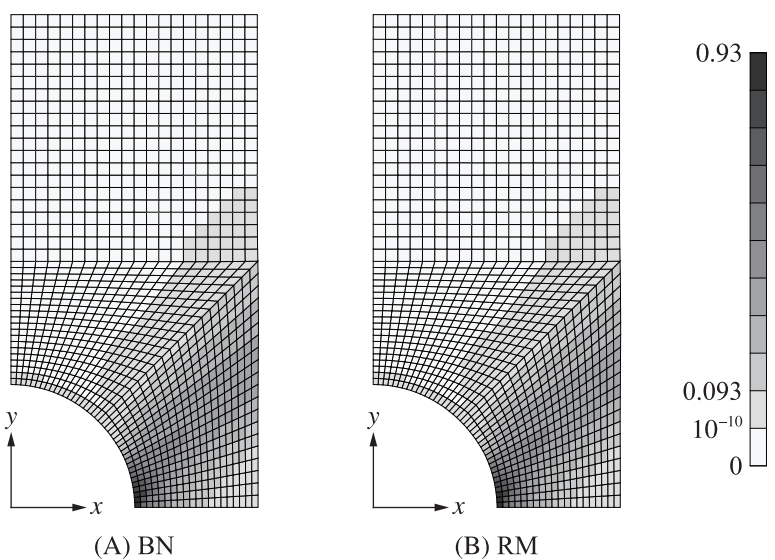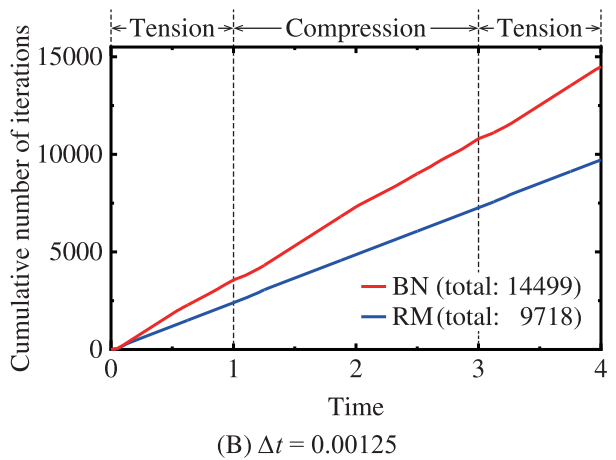
FIGURE 20 Equivalent plastic strain distributions in the final deformation diagram of a plane strain strip of hardening plasticity with a circular hole under cyclic loading for $\Delta t = 0.00125$; (A) BN and (B) RM

(A) BN   (B) RM

(A) $\Delta t = 0.01$ (B) $\Delta t = 0.00125$

FIGURE 21 Cumulative number of iterations for each time step of a plane strain strip of hardening plasticity with a circular hole under cyclic loading; (A) $\Delta t = 0.01$ and (B) $\Delta t = 0.00125$
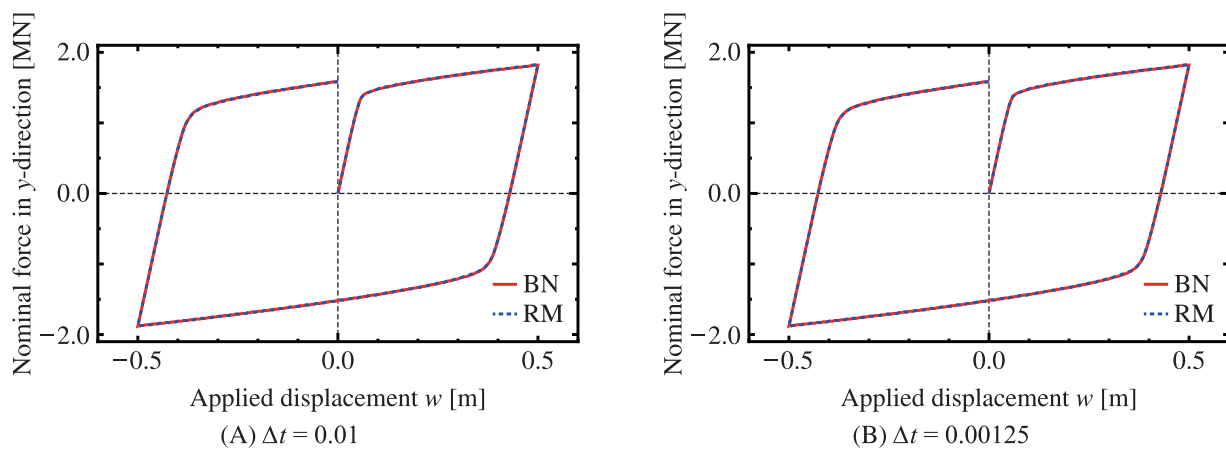
FIGURE 22 Load–displacement curve for a plane strain strip of hardening plasticity with a circular hole under cyclic loading; (A) $\Delta t = 0.01$ and (B) $\Delta t = 0.00125$

Figure 22 illustrates the resulting load–displacement curve in y-direction for the perforated strip under cyclic loading. As shown in Figure 22, the load–displacement curve of the proposed approach coincides with that of the conventional return mapping algorithm. Thus, the proposed approach exhibits robustness as well as the conventional return mapping algorithm even if the case of under the cyclic loading.

5 | CONCLUSIONS

Elastoplastic problems are formulated as a coupled problem of the equilibrium equation and the yield condition at each material point, and a numerical procedure based on the block Newton method to solve the overall structure using the finite element discretization is developed. In the proposed block Newton method, the tangent moduli can be obtained algebraically by eliminating the internal variables, and the internal variables are also updated algebraically without local iterative calculation. In addition, the residual of the yield condition is incorporated into the linearized equilibrium equation. Thus, the proposed approach enables the errors of the equilibrium equation and the yield condition to decrease simultaneously. Although the rate-independent J_2 plasticity is adopted in this study, the proposed approach can be employed for other quasi-static material models. In numerical examples, the number of iterations for convergence at each time step in the proposed approach can be at most one or two more than that in the conventional return mapping algorithm. In the conventional return mapping algorithm, it is inevitable to perform local iterative calculation at each integration point. Though only a two-dimensional model is solved in the numerical examples, the proposed approach can be used for three-dimensional models and other types of finite element, similarly to the conventional return mapping algorithm.

The proposed approach can be applied straightforward to large strain problems and other types of constitutive model with internal variables. Such applications will be investigated in future works.

DATA AVAILABILITY STATEMENT
The data that support the findings of this study are available from the corresponding author upon reasonable request.

ORCID
Takeki Yamamoto https://orcid.org/0000-0003-0373-4723

REFERENCES
1. Hill R. *The Mathematical Theory of Plasticity*. Oxford, UK: Clarendon Press, Oxford University Press; 1950.
2. Koiter W. General theorems for elastic-plastic solids. *Progr Solid Mech*. 1960;1:165-221.

3. Mandel J. Generalisation de la theorie de plasticite de W. T. Koiter. *Int J Solids Struct*. 1965;1(3):273-295.

4. Maier G. A matrix structural theory of piecewise linear elastoplasticity with interacting yield planes. *Meccanica*. 1970;5(1):54-66.

5. Wilkins M. *Calculation of Elastic-plastic Flow*. New York, NY: Academic Press; 1964.

6. Krieg R, Key S. Implementation of a time independent plasticity theory into structural computer programs. In: Stricklin JA, Saczalski KJ, eds. *Constitutive Equations in Viscoplasticity: Computational and Engineering Aspects*. New York, NY: ASME (American Society of Mechanical Engineers); 1976:125-137.

7. Krieg RD, Krieg D. Accuracies of numerical solution methods for the elastic-perfectly plastic model. *J Press Vessel Technol*. 1977;99(4):510-515.

8. Nagtegaal J. On the implementation of inelastic constitutive equations with special reference to large deformation problems. *Comput Methods Appl Mech Eng*. 1982;33(1–3):469-484.

9. Owen D, Hinton E. *Finite Elements in Plasticity: Theory and Practice*. Swansea, Wales: Pineridge Press; 1980.

10. Nayak GC, Zienkiewicz OC. Elasto-plastic stress analysis: a generalization for various contitutive relations including strain softening. *Int J Numer Methods Eng*. 1972;5(1):113-135.

11. Simo J, Taylor R. Consistent tangent operators for rate-independent elastoplasticity. *Comput Methods Appl Mech Eng*. 1985;48(1):101-118.

12. Braudel H, Abouaf M, Chenot J. An implicit and incremental formulation for the solution of elastoplastic problems by the finite element method. *Comput Struct*. 1986;22(5):801-814.

13. Braudel H, Abouaf M, Chenot J. An implicit incrementally objective formulation for the solution of elastoplastic problems at finite strain by the F.E.M. *Comput Struct*. 1986;24(6):825-843.

14. Riggs H. A substructure analogy for plasticity. *Comput Struct*. 1990;37(4):405-412.

15. Martin J, Reddy B, Griffin T, Bird W. Applications of mathematical programming concepts to incremental elastic-plastic analysis. *Eng Struct*. 1987;9(3):171-176.

16. Reddy B, Martin J. Algorithms for the solution of internal variable problems in plasticity. *Comput Methods Appl Mech Eng*. 1991;93(2):253-273.

17. de Borst R. The zero-normal-stress condition in plane-stress and shell elastoplasticity. *Commun Appl Numer Methods*. 1991;7(1):29-33.

18. Chenot J. A velocity approach to finite element calculation of elastoplastic and viscoplastic deformation processes. *Eng Comput*. 1988;5(1):2-9.

19. Ortiz M, Martin J. Symmetry-preserving return mapping algorithms and incrementally extremal paths: a unification of concepts. *Int J Numer Methods Eng*. 1989;28(8):1839-1853.

20. Scalet G, Auricchio F. Computational methods for elastoplasticity: an overview of conventional and less-conventional approaches. *Arch Comput Methods Eng*. 2018;25(3):545-589.

21. Michaleris P, Tortorelli D, Vidal C. Tangent operators and design sensitivity formulations for transient non-linear coupled problems with applications to elastoplasticity. *Int J Numer Methods Eng*. 1994;37(14):2471-2499.

22. Michaleris P, Tortorelli D, Vidal C. Analysis and optimization of weakly coupled thermoelastoplastic systems with applications to weldment design. *Int J Numer Methods Eng*. 1995;38(8):1259-1285.

23. Wisniewski K, Kowalczyk P, Turska E. On the computation of design derivatives for Huber-Mises plasticity with non-linear hardening. *Int J Numer Methods Eng*. 2003;57(2):271-300.

24. Okada JI, Washio T, Hisada T. Study of efficient homogenization algorithms for nonlinear problems: approximation of a homogenized tangent stiffness to reduce computational cost. *Comput Mech*. 2010;46(2):247-258.

25. Zhang L, Li J, Zhang H, Pan S. A second order cone complementarity approach for the numerical solution of elastoplasticity problems. *Comput Mech*. 2013;51(1):1-18.

26. Fritzen F, Hassani MR. Space–time model order reduction for nonlinear viscoelastic systems subjected to long-term loading. *Meccanica*. 2018;53:1333-1355.

27. Miehe C. A multi-field incremental variational framework for gradient-extended standard dissipative solids. *J Mech Phys Solids*. 2011;59(4):898-923.

28. Matthies HG, Steindorf J. Partitioned strong coupling algorithms for fluid–structure interaction. *Comput Struct*. 2003;81(8):805-812.

29. Matthies HG, Niekamp R, Steindorf J. Algorithms for strong coupling procedures. *Comput Methods Appl Mech Eng*. 2006;195(17):2028-2049.

30. Chaboche J, Cailletaud G. Integration methods for complex plastic constitutive equations. *Comput Methods Appl Mech Eng*. 1996;133(1):125-155.

31. Ellsiepen P, Hartmann S. Remarks on the interpretation of current non-linear finite element analyses as differential–algebraic equations. *Int J Numer Methods Eng*. 2001;51(6):679-707.

32. Eckert S, Baaser H, Gross D, Scherf O. A BDF2 integration method with step size control for elasto–plasticity. *Comput Mech*. 2004;34:377-386.

33. Scherf O, Simeon B. Differential-algebraic equations in elasto-viscoplasticity. *Deformation and Failure in Metallic Materials. Lecture Notes in Applied and Computational Mechanics*. Vol 10. Berlin/Heidelberg, Germany: Springer; 2003:31-49.

34. Hartmann S. Computation in finite-strain viscoelasticity: finite elements based on the interpretation as differential–algebraic equations. *Comput Methods Appl Mech Eng*. 2002;191(13):1439-1470.

35. Hartmann S, Wensch J. Finite element analysis of viscoelastic structures using Rosenbrock-type methods. *Comput Mech*. 2007;40:383-398.

36. Netz T, Hartmann S. A monolithic finite element approach using high-order schemes in time and space applied to finite strain thermo-viscoelasticity. *Comput Math Appl*. 2015;70(7):1457-1480.

37. Hartmann S, Bier W. High-order time integration applied to metal powder plasticity. *Int J Plast*. 2008;24(1):17-54.

38. Kullig E, Wippler S. Numerical integration and FEM-implementation of a viscoplastic Chaboche-model with static recovery. *Comput Mech*. 2006;38:1-13.

39. Hartmann S. A thermomechanically consistent constitutive model for polyoxymethylene: experiments, material modelling and computation. *Arch Appl Mech*. 2006;76(5-6):349-366.

40. Hartmann S, Quint KJ, Arnold M. On plastic incompressibility within time-adaptive finite elements combined with projection techniques. *Comput Methods Appl Mech Eng*. 2008;198(2):178-193.

41. Rothe S, Erbts P, Düster A, Hartmann S. Monolithic and partitioned coupling schemes for thermo-viscoplasticity. *Comput Methods Appl Mech Eng*. 2015;293:375-410.

42. Hartmann S. A remark on the application of the Newton-Raphson method in non-linear finite element analysis. *Comput Mech*. 2005;36(2):100-116.

43. Ekh M, Menzel A. Efficient iteration schemes for anisotropic hyperelasto-plasticity. *Int J Numer Methods Eng*. 2006;66(4):707-721.

44. Liu CS. Elastoplastic models and oscillators solved by a Lie-group differential algebraic equations method. *Int J Non-Linear Mech*. 2015;69:93-108.

45. Simo J. Numerical analysis and simulation of plasticity. *Handbook of Numerical Analysis*. Vol 6. B.V.: Elsevier; 1998:183-499.

46. Simo J, Hughes T. *Computational Inelasticity*. New York, NY: Springer-Verlag; 1998.

47. de Souza Neto EA, Peric D, Owen DR. *Computational Methods for Plasticity: Theory and Applications*. Hoboken, NJ: John Wiley & Sons, Ltd; 2008.

48. Voce E. A practical strain hardening function. *Metallurgia*. 1955;51:219-226.

APPENDIX A. RADIAL RETURN ALGORITHM WITH AN IMPLICIT BACKWARD DIFFERENCE SCHEME

In this section, we briefly summarize the algorithm[45,46] based on radial return mapping with an implicit backward difference scheme, which is most commonly used for numerical analyses in elastoplastic problem.

A.1 Radial return mapping

Consider the application of the backward difference scheme to the radial return mapping algorithm within a typical time step $[t_n, t_{n+1}]$. Let $\boldsymbol{n}_{n+1}$ be the unit normal field to the Mises yield surface at the end of a typical time step $[t_n, t_{n+1}]$, and is expressed as,

$$\boldsymbol{n}_{n+1} = \frac{\boldsymbol{\xi}_{n+1}}{\left|\boldsymbol{\xi}_{n+1}\right|}, \tag{A1}$$

the associative variables take the form

$$\boldsymbol{\varepsilon}_{n+1}^{\mathrm{p}} = \boldsymbol{\varepsilon}_n^{\mathrm{p}} + \Delta\gamma\boldsymbol{n}_{n+1}, \tag{A2}$$

$$\boldsymbol{\beta}_{n+1} = \boldsymbol{\beta}_n + \frac{2}{3}H'\Delta\gamma\boldsymbol{n}_{n+1}, \tag{A3}$$

$$\alpha_{n+1} = \alpha_n + \sqrt{\frac{2}{3}}\Delta\gamma. \tag{A4}$$

In addition, the trial state for the prescribed strain deviator $\boldsymbol{e}_{n+1} = \mathrm{dev}[\boldsymbol{\varepsilon}_{n+1}]$ and given $(\boldsymbol{\varepsilon}_n^{\mathrm{p}}, \boldsymbol{\beta}_n, \alpha_n)$ is defined by the following formulae:

$$\boldsymbol{s}_{n+1}^{\mathrm{tr}} = \boldsymbol{s}_n + 2\mu\Delta\boldsymbol{e}_{n+1}$$

and

$$\xi_{n+1}^{\mathrm{tr}} = s_{n+1}^{\mathrm{tr}} - \beta_n,$$

where μ is the shear modulus. Here, the superscript tr indicates quantities evaluated in the trial state. An extension of the argument described above shows that the solution of (9) reduces to the solution of a scalar equation for the consistency parameter $\Delta\gamma$. In view of the relationship $s_{n+1} = s_{n+1}^{\mathrm{tr}} - 2\mu\Delta\gamma n_{n+1}$, the relative stress ξ_{n+1} can be written as

$$\xi_{n+1} = s_{n+1} - \beta_{n+1} = \xi_{n+1}^{\mathrm{tr}} - \left(2\mu + \frac{2}{3}H'\right)\Delta\gamma n_{n+1}. \tag{A5}$$

From the definition $\xi_{n+1} = |\xi_{n+1}| n_{n+1}$ in (A1), the unit normal n_{n+1} is determined exclusively in terms of the trial elastic stress ξ_{n+1}^{tr} as

$$n_{n+1} = \frac{\xi_{n+1}^{\mathrm{tr}}}{|\xi_{n+1}^{\mathrm{tr}}|}.$$

By taking the dot product of (A5) with n_{n+1}, the following scalar (generally nonlinear) equation that determines the consistency parameter $\Delta\gamma$ is obtained as

$$g(\Delta\gamma) = -\sqrt{\frac{2}{3}}\left[\sigma_{\mathrm{Y}} + K(\alpha_{n+1})\right] + |\xi_{n+1}^{\mathrm{tr}}| - \Delta\gamma\left(2\mu + \frac{2}{3}H'\right) = 0. \tag{A6}$$

The solution of (A6) may be effectively accomplished by a local Newton iteration procedure since $g(\Delta\gamma)$ is a convex function, and convergence of the Newton procedure is guaranteed. The details of the local Newton procedure are summarized in Simo and Hughes.[46] Hence, the stress tensor σ is calculated using the solution of (A6) as

$$\sigma_{n+1} = \kappa\left(\mathrm{tr}[\varepsilon_{n+1}]\right)\mathbf{1} + 2\mu\left(e_{n+1} - \Delta\gamma n_{n+1}\right). \tag{A7}$$

A.2 Linearization

The consistent algorithmic elastoplastic tangent moduli can be directly computed by linearization of the two-step return mapping algorithm. These moduli relate incremental strains and incremental stresses and play a crucial role in the overall solutions strategy of the boundary value problem.

A closed-form expression for the elastoplastic tangent moduli can be derived by the exact linearization of the radial return algorithm. By differentiating the algorithmic stress–strain relation in (A7), one obtains

$$d\sigma_{n+1} = \left[\mathbf{C}^{\mathrm{e}} - 2\mu n_{n+1} \otimes \frac{\partial\Delta\gamma}{\partial\varepsilon_{n+1}} - 2\mu\Delta\gamma\frac{\partial n_{n+1}}{\partial\varepsilon_{n+1}}\right] : d\varepsilon_{n+1}, \tag{A8}$$

where $\mathbf{C}^{\mathrm{e}}$ is the elasticity tensor described in (5). To obtain explicit form of (A8), we use following properties[45,46]

$$\frac{\partial n}{\partial\xi} = \frac{\partial}{\partial\xi}\left(\frac{\xi}{|\xi|}\right) = \frac{1}{|\xi|}\left[\mathbf{I} - n \otimes n\right]$$

and

$$\frac{\partial\Delta\gamma}{\partial\varepsilon_{n+1}} = \left[1 + \frac{H' + K'(\alpha_{n+1})}{3\mu}\right]^{-1} n_{n+1}, \tag{A9}$$

which is given by differentiating the scalar consistency condition (A6). In addition,

$$\frac{\partial n_{n+1}}{\partial\varepsilon_{n+1}} = \frac{\partial n_{n+1}}{\partial\xi_{n+1}^{\mathrm{tr}}} : \frac{\partial\xi_{n+1}^{\mathrm{tr}}}{\partial\varepsilon_{n+1}} = \frac{2\mu}{|\xi_{n+1}^{\mathrm{tr}}|}\left\{\mathbf{I} - \frac{1}{3}\mathbf{1} \otimes \mathbf{1} - n_{n+1} \otimes n_{n+1}\right\}, \tag{A10}$$

where

$$\boldsymbol{n} : \boldsymbol{1} = \mathrm{tr}[\boldsymbol{n}] = 0.$$

Substituting (A9) and (A10) into (A8), after some manipulations, the expression of the algorithmic elastoplastic tangent moduli are represented as

$$\mathbf{C}_{n+1}^{\mathrm{ep}} = \kappa \boldsymbol{1} \otimes \boldsymbol{1} + 2\mu \iota_{n+1} \left[\mathbf{I} - \frac{1}{3}\boldsymbol{1} \otimes \boldsymbol{1} \right] - 2\mu \bar{\iota}_{n+1} \boldsymbol{n}_{n+1} \otimes \boldsymbol{n}_{n+1}, \tag{A11}$$

where

$$\iota_{n+1} = 1 - \frac{2\mu \Delta \gamma}{\left| \xi_{n+1}^{\mathrm{tr}} \right|},$$

$$\bar{\iota}_{n+1} = \frac{1}{1 + \frac{[H' + K'(\alpha_{n+1})]}{3\mu}} - (1 - \iota_{n+1}).$$